BSPE 00331-547-5

태평양 심해저 망간단괴의 철-망간 산화광물층의 미세구조 연구

Formation of Fe-Mn Microlayers in Mn-Nodules under the Influence of Oxic Sediment Diagenesis in the NE Equatorial Pacific

1993. 3

한 국 해 양 연 구 소

제 출 문

해양연구소장 귀하

본보고서를 "태평양 망간단괴 철-망간산화광물층의 미세연구" 사업의 최종보고서로 제출합니다.

1993년 3월

한국해양연구소

연구책임자 : 이 경 용
정 갑 식
연 구 원 : 문 재 운
김 기 현
정 희 수

기 술 원 : 지 상 범
연 구 조 원 : 김 채 수

요 약 문

I. 제 목

태평양 망간단괴 철-망간산화광물층의 미세구조 연구

II. 연구내용 및 결과

북동 태평양 적도이북 C-C 지역 서부에 위치한 한국심해연구지역(KODOS)에서 89년과 90년 두 번에 걸쳐 획득한 박스코어 퇴적물과 망간단괴의 광물 화학성분을 분석하여 망간단괴의 형성과 구 기작에 대해 연구하였다. 단괴는 표면구조의 특성에 따라 세가지 유형으로 분류되는 데, 매끈한 표면을 갖는 수성기원의 S 형 단괴는 해저능이나 해저산 지역에서 심하게 생교란된 퇴적층 표면에 노출되어 산출한다. 반면에, 표면이 거친 속성기원의 R 형 단괴는 해저평원지역의 최표층 퇴적물에 부분적으로 혹은 완전히 매몰되어 있다. 이외에도 점이적인 (T) 형의 단괴가 두가지 형의 어느 한가지 형과 함께 산출한다. S 형 단괴는 주상 및 엽리구조를 이루는 vernadite 에 다량의 철과 코발트를 포함하는 반면에, R 형 단괴는 todorokite (buserite)로 구성된 두꺼운 수지상 및 괴상구조에 망간, 니켈, 구리, 아연을 다량으로 함유한다. R 형 단괴들은 S 형 단괴보다 세 배 정도 빠른 속도로 성장한 것으로 계산된다. T 형 단괴들은 R 형과 S 형성분의 중간적인 특성을 보인다. 단괴들은 그 유형이나 형태에 관계없이, 상하부의 화학 및 광물성분의 차이가 뚜렷하여, 상부에는 vernadite, 철 및 코발트가 풍부하고 하부에서는 todorokite (buserite), 망간, 니켈, 구리, 아연, 그리고 퇴적입자들의 함량이 높다.

퇴적물의 성분 및 공극수분석결과에 의하면, 산화환경의 퇴적물중에서도 단괴의 성장이 속성작용에 의해 크게 영향을 받고 있음을 알 수 있다. 속성작

용에 의한 단괴의 성장은 재퇴적한 최상부 표층퇴적물내에서 이루어 지는 데, 이 경우에는 저서생물에 의해 제 삼기 퇴적물에 유입된 유기물이 분해되는 중에 미세망간단괴로부터 재동된 망간, 니켈, 구리 및 아연 등이 todorokite (buserite) 형성에 이용된다. 이러한 작용은 속성기원의 R 형 단괴와 제 삼기 퇴적물, 그리고 미세망간단괴와 todorokite (buserite)의 비슷한 화학성분의 특성으로 알 수 있다. Todorokite (buserite)가 미량금속원소들을 흡수·치환할 수 있는 능력이 제한되어 있어서, 단괴중의 니켈, 구리, 아연의 합함량은 항시 망간의 11% 이하로 제한된다. 퇴적물과 단괴의 이러한 속성작용은 표층해수의 생물생산성에 영향을 받아, 남쪽으로 갈수록 망간의 함량이 높고 크기가 단괴가 산출하며 반면에 생교란된 상부퇴적층에서는 많은 양의 망간이 결핍되어 있다.

Summary

I. Title of Study

Formation of Fe-Mn Microlayers in Mn-Nodules under the Influence of Oxic Sediment Diagenesis in the NE Equatorial Pacific

II. Result

In the Korea Deep Ocean Study (KODOS) area, western part of the Clarion-Clipperton fracture zones, northeast equatorial Pacific, nodules can be classified into three types based on the surface texture. The S-type (hydrogenetic) nodules with smooth surface occur exposed on top of intensely bioturbated sediments of hill and seamount areas. In the abyssal plain, the rough surface, the R-type (diagenetic) nodules are found embedded within the topmost sediment layer. The transitional (T)-type occurs together with either R- or S-types. The S-type nodules are rich in Fe and Co in columnar structures of vernadite, whereas the R-types contain abundant Mn, Ni, Cu, and Zn in dendritic and massive todorokite (buserite) layers. Based on the Mn/Fe ratio, the R-type nodules are estimated to have grown about three times faster than those of S-types. The T-type nodules are intermediate in composition and other characters. Regardless of the type and shape, the tops of nodules are rich in Fe and Co in vernadite, whereas the bottoms contain abundant

Mn, Ni, Cu, todorokite (buserite), and sedimentary clasts with a faster (about 3 times) growth rate.

Analyses of porewater and sediment composition reveal that the growth of nodules by diagenesis is also prevalent within the oxygenated sediments. The diagenetic growth of nodules occurs within the redeposited topmost sediment layer. During biomixing and decomposition of organic materials, Mn, Ni, Cu, and Zn are remobilized from Mn-micronodules and are utilized for the accretion of todorokite (buserite). The chemical composition of micronodules is also similar to those of todorokite (buserite). In the nodules, minor metal species of Ni, Cu, and Zn are concentrated, less than 11% of Mn, due to the limited uptake capacity of todorokite (buserite). In the southern part of the KODOS area, the diagenesis results in large Mn-rich R-type nodules controlled by the surface water productivity. Resedimentation processes of bottom currents and benthic animals also result in the large discrepancy in composition and other characters between the tops and the bottoms as well as the concentric structures.

Contents

List of Figures

List of Tables

INTRODUCTION

In the northeast equatorial Pacific, the growth of manganese nodules is generally attributed to the precipitation of ferro-manganese oxide minerals influenced by either seawater or the underlying sediment (Dymond et al., 1984; Calvert et al., 1987; Skornyakova and Murdmaa, 1992). The influence is variable depending on the characters of nodule-associated sediment that are, in turn, controlled by bottom currents, seafloor morphology, and surface water productivity (Piper and Williamson, 1977; Greenslate et al., 1979; Glasby et al., 1982). Diagenetic nodules are ubiquitous in the abyssal plain area in that the abundance of todorokite, Cu, and Ni increases toward the equator, resulting from the increased biological productivity in the surface water layer (Horn et al., 1973; Calvert and Price, 1977; Skornyakova and Zaikin, 1988; Halbach et al., 1988). These nodules occur partially or embedded within the topmost sediment layer, and are characterized by the abundance of todorokite which forms at a fast rate by utilizing Mn and other minor metals regenerated during diagenesis (Raab, 1972; Bonatti et al., 1972; Halbach et al., 1981; Huh and Ku, 1984). Hydrogenetic nodules are dominant westward due to the increased influence of bottom currents on ubiquitous seamounts extending from the Line Islands Ridge (McKelvey et al., 1979; Skornyakova et al., 1979). Slow precipitation of vernadite and Fe-oxihydroxide results in the concentration of Fe and Co in these nodules which occur generally exposed on the seafloor (Calvert and Price, 1977; Usui et al.,

1979a; Bischoff et al., 1981).

In the Clarion–Clipperton (C–C) fracture zones, nodules are generally classified into three distinct types based on surface texture. Diagenetic nodules are characterized by irregular, rough and gritty surface with microbotryoids (R–type) whereas hydrogenetic nodules show smooth and greasy surface (S–type nodules) (Bonatti et al., 1972; Rabb and Meylan; Halbach et al., 1981). The nodule surface is often transitional, from rough bottom to smooth top surface, or rough partially on the entire surface (tentatively clssified as T–type nodules in this study). The R–type nodules generally show massive and dendrtic structures of todorokite; the S–types are characterized by columnar structures of vernadite (Halbach and Ozkara, 1979; Sorem and Fewkes, 1979 and b; Dymond et al., 1984; Huh and Ku, 1984). The R–type nodules are distinguished by higher Mn/Fe ratio (generally, >4.0) from S–type nodules (Mn/Fe <2.5). The ratio is intermediate in the T–type nodules (Bonatti et al., 1972; Halbach et al., 1981). In the C–C zones, nodule composition is variable with a wide range of the ratio (generally, <7) (Greenslate et al., 1979; Piper and Williamson, 1979; Skornyakova, 1979). The Mn/Fe ratio is immediately related to growth rate of nodules that is, in turn, controlled by sediment diagenesis (Heye and Marchig, 1977; Lyle, 1982; Moore, 1984). The close relationship of types of surface texture to composition and internal structures, although they result from the latest growth processes of nodules, suggest that the formation processes of nodules are relatively uniform (Raab and

Meylan, 1977; Calvert and Williamson, 1977; Halbach et al., 1981; Piper and Blueford, 1982).

Sediment diagenesis is active in the C–C zones, as indicated by an abundance of authigenic minerals such as Fe–rich smectite and micronodules (Greenslate et al., 1979; Hein et al., 1979a and b; Marchig and Gundlach, 1981; Piper et al., 1987). It seems to occur at the sediment–seawater interface by settling and decomposition of organic materials (Klinkhammer, 1980; Bender, 1983; Murray et al., 1984). Biomixing of organic materials with metal–rich older sediment is also regarded to cause episodic and often impulsive regeneration of metals in the topmost sediment part (Muller and Mangini, 1980; Bender, 1983; Emerson et al., 1985). Diagenetic growth seems to occur at a fast rate (up to 200 mm/my) on nodule surface buried within the sediment (Heye et al., 1979; Ku et al., 1984; Lyle et al., 1984; Reyss et al., 1985), resulting in a significant depletion of Mn and other minor metal species in the topmost sediment layer (Greenslate et al., 1979; Bender, 1983; Dymond et al., 1984). During the diagenesis, large portions of Fe ions form smectite combining dissolved silicas within the sediment column (Marchig and Gundlach, 1981; Lyle et al., 1984; Cole, 1985). However, nodule growth by these diagenetic processes has been suspected due to the lack of dissolved metals in the sediment of the C–C zones (Bender, 1971; Boudreau and Scott, 1978; Klinkhammer et al., 1982). Poorness of porewater metals is ascribed to high oxygenating conditions to a depth of sediment column that results from an extremely low sedimentation

rate (Jahnke et al., 1982; Lyle, 1983; Kalhorn and Emerson, 1984; Martin and Knauer, 1984).

In the KODOS area, analyses of mineralogical and chemical compositions of both nodules and the underlying sediment suggest that nodule growth is significantly affected by diagenesis of the uppermost sediment layer. Composition and other characters of nodules appear to be controlled by the burial rates of nodules rather than by the chemical composition of the underlying sediment. Sediment diagenesis occurs mainly during biomixing of settling organic materials and metal-rich older sediment. In turn, bioturbation appears to be stimulated by redeposition of sediment. Largely influenced by the surface water productivity, sediment diagenesis could concentrate larger amounts of some metal species in nodules toward the equator. It may result in an inverse relationship between compositions of nodules and the underlying sediment. Periodic resedimentation could result in a large difference in composition and other characters between types, tops and bottoms, but also in structures of nodules.

Materials and Analytical Methods

The Korea Ocean Research and Development Institute (KORDI) has carried out three cruises for manganese nodule exploration in the Korea Deep Ocean Study (KODOS) area, northeast equatorial Pacific (Fig. 1). At 71 sites, manganese nodules were collected by using either a box corer or free-fall grab samplers. On boards, nodule characters were determined in

detail for number, abundance, size, shape, and surface texture. Nodules were classified into three types of S-, R-, and T-types, depending on the characters of surface textures. Box core sediment was described for color change (Munsell, 1988), bioturbation, lithology, and other characters. At intervals of core depth, sediment for chemical and mineralogical analyses was collected in pre-cleaned polyethylene bottles. Porewaters were squeezed from the sediment of 4 box cores at 0 ° C in a glove box filled with nitrogen.

In the laboratory, manganese nodules that were hardened in resin were halved and photographed for internal structures. In polished sections of 5 nodules, both microstructures and chemical composition in nodules were analysed using a back-scattered electron microphotograph and microprobe (JEOL, JXA-8600). Mineralogical and chemical compositions were determined for 156 bulk nodule samples at 65 sites, and chemical compisition of another 98 nodules was analyzed at 32 sites. Twenty-one samples of Mn-crusts from the seamounts of the Marshall Islands were analyzed for comparison with compositions of nodules. Abundance of mineral species was semi-quantified for 10Å -manganate (todrokite), δ-MnO_2 (vernadite), and aluminosilicate minerals using XRD (Haynes et al., 1982). In this study, 10Å -manganate is classified as todorokite (buserite) due to the changes in X-ray diffraction pattern in that peaks of 10Å and 4.9 Å disappear whereas that of 7 Å becomes more distinctive after heating of nodule powder at 110 ℃ (Fig. 2).

Sediment types were determined based on the amounts of microfossils on smear slides, grain size, and mineralogy. The ages of sediment were assigned by identification of radiolarian and diatom fossils. For three fractions (<2, <1, and <0.1 μm in grain size) of sediment in 26 box cores, clay minerals were analysed by using record of X-ray diffractometer (Phillips, PW-710). Micronodule and smectite were identified by both scanning electron microphotograph and energy dispersive X-ray spectrometer. In porewaters, nutrients were determined by Technicon auto-analyser. Particulate organic carbon in powered sediment was titrated with potasium dichromate and ferrous amonium sulfate. Chemical anaylses of nodule and sediment powders were performed using atomic adsorption spectrometer (Perkin Elmer, IL-251) after complete dissolution in mixed solution of HF, HNO_3, and HCl.

Korea Deep Ocean Study (KODOS) Area

The Korea Deep Ocean Study (KODOS) area is located in the western margin of the C-C zones near the Line Islands Ridge (Fig. 1). The seafloor is deep, generally more than 5,100 m, and slopes gently toward the northwest. It is rather smooth in the eastern part and is rugged with seamounts and knolls in the southern part. The seamounts are mostly steep-sloped, wide (5 to 30 km) and high (400 to 1,500 m), aligned in an E-W trend. They appear to form ridges, following the general bathymetric pattern in the C-C zones. They lack sediment on tops and slopes,

often covered with a thick sediment layer and are complicated with irregular block and step faults. The seafloor basement is also irregular, dissected with numerous faults especially in the eastern part that forms small and large subdued basin floor covered with thin sediment layer. DSDP cores and magnetic anomaly pattern reveal that the basement is 50 to 85 my (middle Eocene to late Cretaceous) old (van Andel et al., 1975). The seafloor is older northwestward and largely offset by a fracture zone which is indistinct in general bathymetric trend. The sedimentary sequence is thick in the southwestern part, comprising an extension of the equatorial sedimentary bulge (Ewing et al., 1968) and the Line Islands Ridge (Normark and Spiess, 1976). In the northeast, the sequence is thin and deformed by basement faults. The sedimentary sequence, especially of the topmost layer, is irregular with various large bedforms and seafloor scours.

MANGANESE NODULES

Types and Occurrence

Three types of nodules occur also in the KODOS area, e.g. R–, S–, and T–type nodules (Fig. 3). The R–type nodules are mostly mononucleated, discoidal, spheroidal or ellipsoidal, whereas S–types are polynucleated and irregular in shape. The T–type nodules are mono– or polynucleated. In box cores, the S–type nodules occur generally exposed on the seafloor. On the other hand, most R–type nodules are partially or embedded in thin topmost sediment layer. Large ellipsoidal or discoidal R–type nodules show equatorial rims (intermediate surface contacting to the sediment/water interface) that are irregular and bumpy with large knobs and small botryoids. The T–type nodules occur together with either the R– or S–types. Nodules generally show distinct orientation of tops and bottoms, of which the latter are associated with the underlying sediment. X–radiographs of sediment cores show that small and large buried nodules of R–types are ubiquitous within thin (<10 cm in thickness) within sediment layer (Fig. 4). The buried nodules generally show a loose outermost layer of Mn–oxide and sediment particles.

Nodules occur in a wide range of water depth (4,600 to 5,500 m). The R–type nodules are dominant (73%) in the abyssal plain; S–type nodules are ubiquitous (29 to 44%) in the seamounts and hills (Fig. 5). The T–type nodules are always found with either R– (12 to 17%) or S–type nodules (3 to 24%). Co–occurrence of three types is uncommon except one site (st. 9028) in the abyssal

plain. Nodules are various in size (a few mm to 20 cm in diameter). Small nodules of less than 4 cm in diameter are accounted 62% in the abyssal plain; more than 80% in the hill and seamount areas. Nodules are larger in the seamount areas than those on the hills due to polynucleation. In the abyssal plain excluding the southeastern part, the R-type nodules are larger in size and are more abundant southward. Nodules are small and mostly R-type that coat thinnly on nuclei of shark's teeth and clay lumps in the southeastern part, showing an immature stage of growth.

Structures and Composition

In nodules, todorokite (buserite) and vernadite comprise major constituents with small amounts of quartz and feldspar (Table 1). Birnessite is rare, except for the nodules with relatively a high Mn/Fe ratio (>5) at sites 9038 and 9039 in the northern abyssal plain. Phillipsite is often found with a large variation (0.0 to 54.3%), especially in nodule core and bottoms. Todorokite (buserite) tends to form massive, dendritic, and cauliflower structures generally in the R-type nodules (Figs. 6-1A to C). Layers of todorokite (buserite) are thick (generally 50 to 100 μm) and are intercalated often with thin (<10 μm) vernadite layers. On the other hand, they are thin and continuous in S-type nodules (Figs. 6-2A to C). Detrital clasts are common especially in the R-type nodules, forming irregular and discontinuous intercalations (Fig. 6-1A). Botryoidal structures of todorokite

(buserite) are found in large pore spaces of nodules (Fig. 6–1B). The S–type nodules are characterized by columnar (pillar) structures which consist of regular and undulating laminations of vernadite (Figs. 6–2A to C). Thin laminations of vernadite occur often on sharp scours and in fissures, similar to those proposed as initial growth stage under the influence of bottom currents (Burns and Burns, 1975; Sorem and Fewkes, 1979). Typical columnar and colloform structures are found in nuclei of S– and T–type nodules (Figs. 6–2A and B). Some nodules show sharp changes of internal structures by scours, i.e., thin laminated to massive to columnar zone toward the surface (Fig. 6–2C). This zonation is attributed to short– and long–period changes of growth by burial and exposure of nodules, resulting from fluctuation of bottom currents (Margolis and Glasby, 1973; Segl et al., 1989; Manigini et al., 1990), or turnovers of nodules themselves (Sorem, 1973; Sorem and Fewkes, 1979; Glasby et al., 1982).

Todorokite (buserite) contains abundant Mn, Ni, Cu, and Zn, generally as much as 2 to 3 times than vernadite (Table 1). Noticeably, Mn is most abundant (up to 59.4%) with small amounts of Fe (less than 1%) in massive and cauliflower structures, also in intercalated thin layers of todorokite (buserite) in columnar structures (Figs. 6–1D and –2D). On the other hand, vernadite is rich in Fe and Co. A ternary relation of Fe, Mn, and 10·(Cu+Ni+Co) (Fig. 7) suggests that todorokite (buserite) results from sediment diagenesis, whereas vernadite forms by hydro–

genetic growth (Sorem and Fewkes, 1979; Usui, 1979). Concentration of minor metals (Ni, Cu and Co) is always less than 16% of Mn in the two minerals. Chemical characters of the two minerals are governed by Mn/Fe ratio, which is larger in todorokite (buserite) as much as 17 times on the average than that in vernadite (Table 1). In todorokite (buserite), sum of Cu and Ni increases to the maximum (5.35%) at about 21 of Mn/Fe ratio, and decreases to more or less a uniform value (4 to 4.5%) (Fig. 8A). Less amounts of Ni and Cu are encountered especailly in Mn-rich (>40%) todorokite (buserite), similar to those in a variety (birnessite) of todorokite (buserite) (Usui, 1979; Reyss et al., 1982; Giovanoli and Arrhenius, 1988). Distribution of Zn content is similar to that of Ni+Cu. Cobalt content decreases exponentially to the minimum value (0.1%) at about 20 of the Mn/Fe ratio in todorokite (buserite) and variable (0.05 to 0.70%) in vernadite (Fig. 8B). It tends to increase linearly as Fe content increases up to 20% in the two minerals and decrease sharply in vernadite with more than 20% Fe (Fig. 9).

In nodules, Mn and Fe comprise dominant metal species. The R-type nodules are characterized by high ratio of todorokite (buserite)/vernadite that comprises concentration of Ni, Cu, and Zn (Table 1). On the other hand, the S-types contain abundant Fe and Co in vernadite. The T-type nodules are intermediate in composition between the two types. The amounts of detrital minerals decrease proportionally from S-, T-, to R-type nodules. Manganese crusts consist mostly of vernadite (91.5% peak

intensity on the average), and are characterized by an abundance of Fe (15.2% on the average) and Co (0.53%). Compared to those in the C–C zones, the nodules contain more Fe and Co, whereas less Mn, Ni, Cu, and Zn. This is probably due to larger influence of bottom currents in the KODOS area, near the Line Islands Ridge (McKelvey et al., 1979; Skornyakova, 1979; Friedrich et al., 1988). A ternary relationship of Mn, Fe and 10·(Cu+Ni+Co) (Fig. 10) indicates that the R–type nodules are diagenetic, whereas the S–types are hydrogenetic in origin (Bonatti et al., 1972; Calvert and Price, 1977; Halbach et al., 1981). The T–type nodules show mixed influences of both seawater and the underlying sediment (Rabb, 1972; Moritani et al., 1977; Reyss et al., 1985). The Mn/Fe ratio (0.9 to 2.1) of Mn–crusts is similar to that in the seawater beneath the oxygen minimum depth (Qunby–Hunt and Turekian, 1983), suggesting that they are pure hydrogenetic product (Hein et al., 1988). Both the ratios of Mn/Fe and todorokite (buserite)/vernadite are larger southward toward the equator. These characters comprise the previous findings in the C–C zones (Calvert et al., 1978; Piper and Williamson, 1978; Piper and Blueford, 1982). The sum of Cu and Ni contents increases to the maximum value (about 3 %) and is more or less uniform beyond about 5 of Mn/Fe ratio (Fig. 11A). It is similar, although less distinctive, to the reversed concentration of these metals in nodules where sediment diagenesis is active (Friedrich et al., 1983; Halbach et al., 1988). On the other hand, Co content decreases from about 0.4% to a constant value of about 0.1% at larger than

2 of the ratio (Fig. 11B).

The growth rate of nodules and mineral species can be estimated by using the equation of Huh and Ku (1984), which is based on an immediate relation of growth rate to Mn/Fe ratio (Heye and Marchig, 1977; Piper and Williamson, 1977; Lyle, 1982). Todorokite (buserite) seems to accrete at a fast rate (36 mm/my, on the average), about 13 times than that (2.8 mm/my) of vernadite (Table 1). In the case of Mn-rich (>40%) and Fe-poor (<1%) todorokite (buserite), the growth rate is impetus, faster than 1000 mm/my, as determined by Finney et al. (1984). Average growth rate is estimated as 9.1 mm/my in the R-type, 4.7 mm/my in the T-type, and 3.0 mm/my in the S-type nodules, respectively. These values range in general growth rates (1 to 10 mm/my) of nodules in the Pacific (Ku and Broecker, 1966; Moore et al., 1981; Mangini et al., 1990). Manganese crusts appear to have grown at a slow rate of lower than 1 mm/my.

Inter-metal relations in Mn-nodules

Inter-metal relations were obtained using varimax R-mode factor analysis. In the two Mn-oxide minerals, metals are statistically classified into 3 groups: Mn-Cu-Ni-Mg, Fe-Co-P, and Al-Si (Table 2a). It indicates that nodular minerals consist of metals associated with Mn-, Fe-oxides, and alluminosilicates (Bischoff et al., 1981; Moorby and Cronan, 1981). The former two groups are inversed in interrelations. Aluminum and Si are related to other metals with a moderate relation to Mg. In vernadite,

the metals of the first group are significantly related to Mn/Fe ratio; those of the second group are affinitive to Mn–Ca–Si–Ti. These characters may imply that the accretion of vernadite is also largely influenced by the underlying sediment (Li, 1984; Calvert and Piper, 1984). It is generally believed that Co incorporates into vernadite by ionic exchange with excess Mn and often Fe ions in high oxidation conditions (Piper et al., 1984; Giovanoli and Arrhenius, 1988). However, its concentration is significantly limited in the case of larger (>20%) amounts of Fe (Fig. 9).

In nodules, transition metals occur preferentially in two groups; Mn–Cu–Ni–(Zn) and Fe–Co (Table 2b). The former are closely related to Mn/Fe and todorokite (buserite)/vernadite ratios in all the types of nodules. The latter are considerably related to the abundance of detrital clasts and the two ratios in S– and T–type nodules. Interrelations of Fe–Mn–Co are distinct in S–types, similar to those in vernadite. Generally, Co is associated with Fe in the R–types; Fe–Mn oxides in the S–type nodules of the Pacific Ocean (Calvert and Price, 1977; Greenslate et al., 1979; Halbach and Ozkara, 1979). The increase of todorokite (buserite) and detrital clasts compensates the abundance of Fe and Co, from S–, T–, to R–type nodules (Table 1). The chemical composition of Mn–crusts is dominated by the interrlation of Mn–Fe–Co (Table 2c). The amounts of hydrogeneous materials in the T–type nodules seem to be negligible, as indicated by less significant relations of Fe and Co to other metals. It is generally knwon that the metals of Fe and Co are hydrogenetic origin (Moorby and

Cronan, 1981; Dymond et al., 1984; Piper, 1988). Halbach et al. (1981) estimated the portion of hydrogenetic materials to be 20 to 40% in their mixed type of nodules.

SEDIMENT

General Characters

Bulk sediment is mostly classified into radiolarian-bearing smectitic clay, often siliceous clay (siliceous fossils, 15% to 30%). Also siliceous ooze (st nos., 8904, 9032) and nannofossil ooze (st nos., 8906 and 9012) occur with abundant fossils (more than 80%), underlying unit 1 (Fig. 12). These oozes occur at about 5,000 m in water depth, comprising depressed CCD (Piper, 1988) in the KODOS area. The topmost sediment column in the KODOS area comprises either zeolitic clay or siliceous ooze where radiolarian-bearing clay is dominant (clay fraction, more than 70%), often with calcareous ooze. It is divided into two or three units, based on distinct color change, bioturbation, lithology and mass physical properties (Fig. 12). The topmost unit 1 is dark yellowish or reddish brown (10YR3/4 to 5YR3/3, Munsell, 1988), homogeneous, bioturbated, and thin (mostly, <10 cm in thickness). The boundary between unit 1 and the lowermost unit 3 is transitional, often sharp by truncation of large burrows within the lower sediment layer. Unit 1 comprises "peneliquid layer" of Halbach and Ozkara (1979) and "mixed layer" of Berger et al. (1979), i.e., water-saturated (water content, >300%) and cohesionless. Unit 2 is generally dark brown in color (10YR3/3 to 5YR 3/2), mottled with simple and large haloed burrows, and variable in thickness. It is intermediate in sediment characters between the topmost and lowermost units (transitional layer, Berger et al., 1979). The third unit is dark brown in color (5YR3/1 to 10YR4/2) and less

bioturbated, corresponding to the "historic layer" (Berger and Killingley, 1982). In the topmost unit (unit 1), burrows are small (<1 mm in diameter) and generally indistinguishable, whereas they are large (mostly, about 4 cm in diameter) in the lower units. Burrows are most well preserved in unit 3, which are often intersected by smaller burrows filled with the overlying sediment and fecal pellets. They are distinguished by light yellow-colored haloes (Berger et al., 1979) around which sediment is often darker, due to manganese-rich particles of micronodules (Fig. 12, core no., K9032) .

In core sediment, early Eocene (often Paleocene) to Quaternary radiolarians are ubiquitous (as much as more than 10% of bulk sediment) and mixed at various rates in units 1 and 2. Unit 1 is assigned to the Quaternary and the lower units to the Tertiary (early Eocene to Pliocene), based on radiolarians and diatoms. Often, only late Quaternary (Holocene) radiolarians are found in unit 1, overlying the Oligocene to Miocene nannofossil calcareous ooze (Fig. 12). The amounts of Quaternary radiolarians in unit 1 increase from less than 10% to more than 80% of total radiolarian assemblage southeastward, reflecting the influence of primary production in the surface water (Quinterno and Theyer, 1979; Wolfart, 1988). The ages of Tertiary sediment is older northwestward (Fig. 13). Both radiolarian and diatom fossils reveal that sedimentation rate is less than 0.2 mm/10^3 yrs for the Tertiary sedimentary layer, similar to those obtained by others in the C-C zones (Listzin, 1972; Krishnaswami, 1976). The lowered

sedimentation rate is probably due to more extensive erosion and dissolution of sediment by inhanced bottom currents (Johnson, 1974; Normark and Spiess, 1976; Wolfart, 1988). Assuming that the layer were deposited for the last 7,000 yrs, the accumulation rate during the Quaternary is estimated to be about 15 mm/10^3 yrs. The rate is consistent with that (8 to 25 mm/10^3 yrs) of the topmost mixed layer in the northwestern margin of the equatorial zone (Marchig and Gundlach, 1979; Berger and Killingley, 1982; Lyle et al., 1988).

Composition

Surface sediment consists mainly of clay (70–90%) with minor amounts (<30%) of sand– and silt–size fossil (dominantly of radiolaria) fragments. The coarse (>62 μm) particles consist of micronodules with minor amounts of smectite in less–bioturbated Tertiary sediment (Fig. 14). Trace amounts (<5%) of volcanic (or opaque) and quartz detritus are also encountered. Micronodule is concentrated often in the outer margins of haloed burrows where the Quaternary sediment layer is thin (core no., 9032). Micro–nodules consist mostly of Mn with subsequent amounts of Fe, similar to todorokite (buserite) in nodules (Table 3). Smectite contains 5 to 9% Fe, ranging in values documented in other areas (Aoki et al., 1979; Hein et al., 1979b). Energy dispersive X–ray (EDX) spectrum of a smectite grain is characterized by distinctive peaks of Si, Al, and Fe (Fig. 15), similar to that of nontronite (Welton, 1984).

In clay fractions (<2 μm), smectite and illite are major

constituents with minor amounts (<20%) of kaolinite and chlorite (Fig. 16). Smectite is most abundant (>70%) in unit 3, whereas illite is enriched in the uppermost part. The abundance of these minerals is variable with a wide range (30 to 80%) in units 1 and 2, whereas it is relatively uniform in the third unit. Terrigenous component is more abundant (>50%) in the hill and seamount areas and in younger (Pliocene) sediment, whereas smectite is abundant (50 to 98%) in older sediment in the abyssal plain. Size fractionation of smectite from illite is distinctive; it is more abundant in the finer (<0.1 and <1 μm) sediment of the upper two units. In the lowermost Teritary sediment, smectite is abundant and independent of grain size. Ths amounts of smectite increase northward, probably due to the prolonged diagenesis and reworking of sediment.

Porewater Nutrients

In four box core sediment, the abundance of porewater nutrients and total particulate organic carbon (POC) increases progressively southward (Fig. 17). The POC decreases linearly downcore, with a mixmum concentration (0.7–0.8%) in the topmost sediment. Nitrate+nitrite, mostly of nitrate (98%) (Jahnke et al., 1982), is about 40 to 115 μM, more than that (33 to 37 μM) in the near–bottom seawater in the C–C zones (Muller and Mangini, 1980, Klinkhammer et al., 1982). Phosphate content is generally less than 3 μM. Silica is dissolved in a range of 100 to 300 μM, similar to the values determined in siliceous sediment

(Klinkhammer et al., 1982). It is about twice higher than that in seawater (Callender and Bowser, 1980; Jahnke et al., 1982). Generally, nutrients decrease upward to the surface within a few cm depth, below which they are more abundant and increase downcore. Their abundance is clearly opposite to that of POC. Some variations occur at the boundary between units and in large burrows. These distributional characters of nutrients are common in deep sea sediment which are oxygenated at depth, especially in the northeast equatorial Pacific (Bourdreau and Scott, 1978; Hartman and Muller, 1982; Sawlan and Murray, 1983; Emerson et al., 1985).

Downcore increase of nutrients (especially of nitrate) in porewater (Fig. 17) suggests that decomposition of organic matters (nitrification) is active due to sufficient amounts of dissolved oxygen within the sediment (Emerson et al., 1980; Murray and Grundmanis, 1980; Emerson et al., 1985; Lyle et al., 1988). This process is more active to the south, resulting in a larger variation of POC and more abundant nutrients downcore. In the topmost sediment layer, depleted nutrients and abundant POC indicate that nutrients are removed to the overlying seawater as soon as organic matters accumulate (Schink and Guinasso, 1978; Jahnke et al., 1982; Bender, 1983). Below the layer, variable abundance of nutrients (especially of nitrate) in large burrows results probably from intermittent and rapid introduction of organic matter–rich topmost sediment (Berner, 1980; Prahl et al., 1989). In the C–C zones, the sediment is oxygenated to a depth as revealed by redox

potential higher than 400 mV up to 10 m depth (Hartmann and Muller, 1982). Klinkhammer et al. (1982) also documented that suboxic reduction of metal oxides occurs unlikely at least within 50 cm depth of sediment column at Manganese Nodule Project (MANOP) Site S (Klinkhammer, 1980; Bender, 1983).

Transition Metals

The concentration of transition metal elements (Fe, Mn, Cu, Ni, Co, and Zn) in box core sediment are variable (Fig. 18), depending on the sediment type and age; Tertiary sediment (unit 3) is rich in metals as much as 2 to 3 times than the topmost unit 1 (Quaternary), and 4 to 10 times than siliceous and calcareous oozes. In intensely bioturbated unit 2, the abundance of metals is more or less similar to that in unit 1. However, Fe and Co contents are generally uniform downcore. These characters comprise those documented in the Pacific pelagic sediment which is sufficiently oxygenated to a depth (Calvert et al., 1978; Stoffers et al., 1982; Piper, 1988). The abundance of micronodules comprises peaked concentrations of Mn and other minor metals at the boundaries between units and in the lowermost Tertiary sediment. The distributional pattern of metals is also controlled by bioturbation, similar to that of clay minerals (Fig. 16). In sediment, Mn/Fe ratio is variable from 0.04 to 0.60; generally less than 0.2 in the upper two units, 0.15 to 0.40 in the third unit. On the other hand, the ratio of Cu+Ni+Zn/Mn is larger (0.10–0.32) in the two upper units than in the lowermost unit (0.10–0.16).

Average Mn/Fe ratio of the topmost (unit 1) sediment increases progressively northward, whereas Cu+Ni+Zn/Mn ratio increases southward (Fig. 19). These characters indicate that diagenetic products, probably of micronodules, are more abundant in older sediment (Figs. 14 and 15) (Calvert et al., 1978; Kalhorn and Emerson, 1984).

An analysis of intermetal relation shows that the metals are classified into two groups; Fe–Co (correlation coeff., 0.65) and Mn–Cu–Ni–Zn (>0.72) (Table 4). Cobalt content is also correlated with the latter (0.50 to 0.72), whereas Zn shows some affinity to the former metals (0.62 to 0.63). The former show positive relations with terrigenous clay minerals, whereas no or little relation with Mn/Fe ratio and smectite content. Especially, smectite content is inversely proportional (−0.94 to −0.99) to the abundance of illite, kaolinite, and chlorite. These characters imply that the sediment composition is mainly determined by authigenic processes with a subsequent influence of detrital clasts (Halbach et al., 1981; 1988; Li, 1982). According to sequential leaching of the Pacific pelagic sediment (Krishnaswami, 1976; Forstner and Stoffers, 1981), large portions of Mn, Ni, Cu, Co and Zn are found in chemically soluble fractions and micronodules; Fe is mostly held in insoluble detrital grains or in less–soluble hydrous oxides and smectite with small amounts of minor metals (Table 3) (Krishnaswami, 1976; Piper and Williamson, 1977; Graybeal and Heath, 1984; Emerson et al., 1985).

DIAGENETIC GROWTH OF Mn-NODULES

In both sediment and nodules, statistical analysis shows that metal species co-occur preferentially in two groups; Mn-Ni-Cu -Zn and Fe-Co (Table 2 and 4). These fractionations of metals are due to the post-depositional diagenesis that redistributes the metal species between sediment and nodules (Krishnaswami, 1976; Halbach et al., 1979; Li, 1982; Calvert and Piper, 1984). In nodules, the former metals are concentrated in todorokite (buserite) (Table 1) that are regenerated from the underlying sediment, whereas the latter are abundant in vernadite and Fe-oxihydroxide precipitated directly from seawater (Raab, 1972; Calvert and Price, 1977; Froelich et al., 1981; Reyss et al., 1982). The upward migration of Ni, Cu, and often Zn is confirmed by analyses of sediment porewater at various nodule sites, although dissolved Mn is more or less similar to that in the bottom water (Klinkhammer, 1980; Callender and Bowser, 1980; Klinkhmmer et al., 1982; Bender, 1983; Sawlan and Murray, 1983). Porewater Co seems to behave similar to Fe (Lyle et al., 1984; Aplin and Cronan, 1985). The relative significance of the two sources of metal species controls the characters of composition and structures of nodules that are immediately related to the types of surface textures (Table 1).

The types and composition are closely related to the buried portion of nodules, rather than to the chemical characters of the topmost Quaternary sediment (Fig. 20). This relation confirms that the diagenetic accretion of nodules takes place in less

oxygenated conditions of redeposited sediment (Halbach and Ozkara, 1979; Giovanoli and Arrhenius, 1988; Takemastu et al., 1988). Todorokite (buserite)-rich R-type nodules generally occur partially or embedded within the sediment (Fig. 3) with wide ranges of Mn/Fe and Ni+Cu+Zn/Mn ratios (Fig. 20B). On the other hand, vernadite-abundant S- and T-type nodules are found exposed on the top of sediment with small Mn/Fe (<0.15) but large Ni+Cu+Zn/Mn ratios (>0.11). These indicate that the S- and T-type nodules are also affected by sediment diagenesis. Vernadite and Fe-oxihydroxide could uptake some amounts of minor metals in the bottom water layer that are diffused from the underlying sediment (Calvert and Piper, 1984). In this case, the chemical composition of hydrogenetic (S-type) nodules is similar to the hydrogenous fractions of the underlying sediment (Calvert et al., 1978; Piper, 1988). The proportion of hydrogenous materials decreases from S-, T-, to R-type nodules (Fig. 10), as the buried portion of nodules increases (Fig. 3). Exposure of S-type nodules on the seafloor of hill and seamount areas results from active resedimentation processes of benthic animals and bottom currents. Active resedimentation processes are evidenced by abundant Tertiary fossils in the topmost Quaternary sediment layer (Moore, 1970; Quinterno and Theyer, 1979). Long term burial and exposure of nodules form respectively thick and massive todorokite (buserite), and vernadite-rich columnar zones (Fig. 6-2C), as suggested earlier (Margolis and Glasby, 1973; Halbach and Ozkara, 1979; Segl et al., 1989; Mangini et al., 1990). The chemical

composition of nodules is dependent on the relative uptake ability of minor metal species in the two major Mn–oxide minerals. The sum of Ni, Cu, and Zn is alway less than 11% of Mn abundance in nodules (Fig. 20A), resulting from their limited concentration less than 16% of Mn in the two minerals (Fig. 7) (Usui, 1979; Giovanoli and Arrhenius, 1988; Takematsu et al., 1988).

In the KODOS area, the uppermost sediment layer is oxygenated enough to decompose organic materials to a depth, as shown by downcore–increasing porewater nutrients (Fig. 17). Within such conditions, remobilization of metals is unlike to occur due to rapid incorportaion of metal ions into sedimentary phases by reoxidation (Bonatti et al., 1971; Klinkhammer et al., 1982; Emerson, 1980; Lyle, 1983). However, the inverse relation of chemical composition of nodules to that of the underlying sediment (units 1 and 2) (Fig. 20) is strongly suggestive of the nodule growth by post–depositional diagenesis that is active. Unit 1 sediment (Quaternary) are intermediate in chemical characters between the lower units, resulting from admixture of the Tertiary sediment components in variable amounts by reworking processes (Piper, 1988). The inverse relation is most distinctive between the compositions of nodules and unit 2 sediment, indicating that diagenesis takes place more efficiently during bioturbation (Piper, 1988), rather than oxic decomposition of organic materials at the sediment–seawater interface (Emerson et al., 1980; Klinkhammer et al., 1982; Sawlan et al., 1983). According to Callender and Bowser (1980), dissolved metal species are most abundant in the

mottled sediment zone (Jahnke et al., 1982; Lyle et al., 1984). In this case, the growth of nodule using the metals results in sharp depletion of micronodules and some metal species in the upper units 1 and 2 sediment (Figs. 14 and 18). The concentration of minor metals of Ni, Cu, and Zn, less than 0.11% Mn, is controlled by micronodules (Fig. 20B), as in nodules by todorokite (buserite) (Fig. 7). Micronodule is regarded as a species of todorokite (buserite), the major product of Mn reoxidation (Piper et al., 1987; Sugisaki et al., 1987; Friedrich et al., 1988). Remobilization and reoxidation of metals seem to be episodic and often impulsive, as indicated by impetus growth rate (>1,000 mm/my) of todorokite (buserite). Within the oxygenated sediment, labile organic materials are rapidly decomposed during bioturbation (Paul et al., 1978; Smith and Baldwin, 1984; Chester, 1990), resulting in variable distribution of metals, nutrients, and POC (Figs. 16 and 17). The concentration of micronodule in the outer margin of haloed burrows in units 2 and 3 (Fig. 12, core no., K9032) is ascribed to rapid reoxidation of Mn and other minor metal ions regenerated by decomposition of organic materials within the burrows (Piper et al., 1987; Lallier–Verges and Alberic, 1989).

In the KODOS area, the influence of surface water productivity on diagenesis is clearly appeared by southward enrichment of Ni, Cu, and Zn relative to Mn in nodules and the underlying sediment (Fig. 20). The diagenesis of the underlying sediment could be also enhanced by the increased accumulation of labile organic materials, as shown by southward decreasing Mn/Fe

ratio. Porewater nutrients also increase southward (Fig. 17), comprising the amounts (10 to more than 80%) of the Quaternary radiolarian fossils. As the result of diagenesis, the R-type nodules are abundant and larger with lower todorokite (buserite)/vernadite, constant Ni+Cu+Zn/Mn, and larger Mn/Fe ratios in the southern part. These characters seem to be due to fast growth of nodules by excess uptake of Mn relative to minor metals (Turner and Busseck, 1981; Piper et al., 1984). The higher Cu+Ni+Zn/Mn ratio is probably due to active remobilization of Mn that is caused by high accumulation rate of biogenic materials near the equatorial production zone (Piper and Williamson, 1977; Halbach et al., 1981; Martin and Knauer, 1984). Manganese-rich todorokite (buserite) (birnessite) tends to form in suboxic conditions of hemipelagic sediment beneth the productive surface water (Halbach et al., 1981; Reyss et al., 1985). Some amounts of birnessite are found in nodules with relatively a large Mn/Fe ratio at sites 9032 and 9038. In the C-C zones, the surface water productivity is variable with an order of 2 to 3 in the magnitude of organic carbon flux, depending on locations and seasons (El-Sayed and Takuchi, 1979; Fisher, 1984). These conditions could cause Mn-rich todorokite (buserite) to accrete at an impetus rate (Table 1) (Heye and Marchig, 1977; Finney et al., 1984; Reyss et al., 1985). In the northern part of the KODOS area, nodules are small and contain more vernadite, although they are R-typed and occur in older Tertiary (mostly of Eocene) sediment (Fig. 13). These nodules result propbably from the barren influence of surface water

productivity since the initiation of growth. Here, weak diagenesis of sediment is indicated by abundant micronodules (Fig. 14), small amounts of organic materials (POC) (Fig. 17), and higher Mn/Fe ratio (Fig. 19).

DISCUSSION

The growth of nodules by sediment diagenesis has been progressively proposed in oxygenated pelagic sediment (Greenslate et al., 1979; Lyle et al., 1982; 1984; Marchig et al., 1979; Dymond et al., 1984; Kalhorn and Emerson, 1984). However, it is still suspected because porewater metals are poor in siliceous oozes and red clays with an extremely low sedimentation rate (Boudreau and Scott, 1978; Hartmann and Muller, 1982; Klinkhammer et al., 1982; Murray et al., 1984). In these cases, the growth of nodules has been often ascribed to occasional exposures to seawater (Boudreau and Scott, 1978; Krishnaswami and Cochran, 1978). In the KODOS area, diagenetic growth of nodules could be confirmed by the mirror relationship between the compositional characters of nodules and the underlying sediment (Fig. 20). Southward increase in sediment diagenesis comprises progressive depletion of Mn, Ni, Cu, and Zn, increase of particulate organic carbon (POC), and porewater nutrients in the uppermost sediment layer (Figs. 17 and 18). These characters are strongly indicative of nodule growth by utilizing Mn and minor metals removed during the sediment diagenesis under the significant influence of surface water productivity. During the diagenesis, Mn is removed at a faster rate than those of other metals species (Bonatti et al., 1971), resulting in the increase of Ni, Cu, and Zn, whereas the decrease of Mn/Fe ratio in the underlying sediment (Fig. 20B). In both margins of the equatorial zone of the Pacific Ocean, these characters are generally ascribed to the accumulation of nodular

metals released by active dissolution of biogenic materials beneath the CCD (Greenslate et al., 1979; Horn et al., 1973; Elderfied, 1976). Compared with the Mn-crusts of the Marshall Islands (Table 1) where the surface water layer is barren (Hein et al., 1988), the S-type nodules contain Cu, Ni, and Zn as much as about 1.6 times with the faster grwoth rate of three times. The precipitation of vernadite can concentrate Cu and Ni in the S-type nodules that are preferentially associated with the biogenic materials (Bischoff et al., 1981; Calvert and Piper, 1984; Dymond et al., 1984). The abundance of some metal species in the bottom water is also attributed to sediment resuspension and metal diffusion from the seafloor (Baker et al., 1979).

Diagenetic growth of nodules seems to be enhanced by selective reduction of micronodules during early sediment diagenesis, although the significance of micronodules is still debateful (Forstner and Stoffers, 1981; Marchig and Gundlach, 1981; Piper, 1988). In the lowermost Tertiary sediment, Mn and minor metals are abundant as much as 2 to 3 times that those in the uppermost sediment (Fig. 18), consistent with the distribution of micronodules (Fig. 14). These amounts of metal fractions are regarded to be sufficient for nodules to grow at a rate of up to 300 mm/my (Lyle et al., 1984; Kalhorn and Emerson, 1984; Mangini, 1988). On the other hand, hydrogenous metal species of Fe and Co are relatively uniform downcore (Fig. 18). The large portions of Fe are utilized for the formation of smectite by chemical reaction of Fe-oxyhydroxides and silicas dissolved from

siliceous fossils in oxygenating conditions (Aoki et al., 1979; Johnson, 1976; Hein et al., 1979b; Cole, 1985). Smectite seems to be formed at a fast rate, as shown by more abundant fine-grained fractions in the the upper sediment units 1 and 2 (Fig. 16). Controlled by micronodules, the chemical characters of Tertiary sediment are similar to those of R-type nodules, i.e., more or less a constant value (approximately 0.11) of Ni+Cu+Zn/Mn as Mn/Fe ratio increases (Fig. 20B). Micronodule is analogous in chemical composition to todorokite (buserite) (Tables 3). These are indicative of that micronodules are an important carrier of metals from the lowermost Tertiary sediment to the overlying nodules (Lyle et al., 1984; Moore, 1984). The remobilization of metals from micronodules occurs during biomixing and decomposition of organic materials (Berner, 1980; Janke et al., 1982; Piper, 1988), as shown by large depletion of metal species and micornodules to depth which bioturbation reaches (Figs. 14 and 18). These processes can be evaluated as the transportation of metals for the nodule growth which takes place without the sufficient supply of metals through interstitial waters (Berner, 1980; Lyle et al., 1984; Moore, 1984; Reyss et al., 1985). Small and rare R-type nodules in older (Eocene) sediment of the northern part are due to less influence of sediment diagenesis. Here, higher Mn/Fe ratio is indicative of highly oxygenated conditions of sediment, probably comprising abundant micronodules (Figs. 14 and 19). Porewater nutrients are also poor (Fig. 17), resulting from an extremely low sedimentation rate far

beyond the influence of the equatorial production zone. These findings are quite different from others that nodule growth is enhanced by either metal-rich bottom currents (Piper and Blueford, 1982; Calvert and Piper, 1984; Calvert et al., 1987) or regeneration of the metals retained in the redeposited Quaternary sediment (Skornayakova and Murdmaa, 1992).

Different from those with smooth and greasy surface in hemipelagic sediment (Halbach et al., 1981; Reyss et al., 1982; 1985), rough and gritty surface textures of R-type nodules are often attributed to the direct accretion of todorokite (buserite) grains that formed already within the sediment (Heye et al., 1979; Mangini et al., 1988; Chester, 1990). In this case, the nodules should be similar in chemical characters to the underlying sediment, in contrast to those found in the KODOS area (Fig. 20B). Rough surface textures could be ascribed to the rapid and episodic accretion of todorokite (buserite), similar to that of micronodules in the more oxygenated outer margin of haloed burrows (Fig. 12, st. 9032) within which organic materials decay (Piper et al., 1987; Lallier-Verges and Alberic, 1989). The organic materials decay at a fast rate in the deep seafloor due to the low sedimentation rate and oxygen-saturated bottom water (Paul et al., 1978; Smith and Baldwin, 1984; Chester, 1990). These processes may be indicated by the outermost loose layer of buried nodules in the oxygenating conditions within the sediment (Fig. 4). In nodule surface, microorganisms seem to induce favorable conditions for remobilization and reoxidation of Mn ions

(Dugolinsky et al., 1977; Thiel and Schneider, 1988). The role of microbial mediation for accretion of todorokite (buserite) has been appreciated by laboratory experiments (Takematsu et al., 1988).

CONCLUSIONS

Analyses of compositions of nodules and the underlying sediment reveal that nodule growth is largely controlled by sediment diagenesis. The influence of diagenesis is proportional to the burial rate of nodules; stronger from S–, T– to R–type nodules, resulting from the effects of resedimentation processes of bottom currents and benthic animals. These characters also reflect that diagenetic growth occurs on nodule surface buried within the redeposited sediment. Resedimentation processes appear to be most responsible for the large discrepancies in compositions and other characters between tops and bottoms, but also in structures of nodules. Diagenetic growth of nodules takes place by accretion of todorokite (buserite) using Mn, Ni, Cu, and Zn that are easily regenerated from micronodules contained in lowermost Tertiary sediment. In this case, bioturbation plays an important role for inducing sediment diagenesis by mixing organic materials into oxygenated older sediment. Some amounts of diagenetic materials in S–type nodules is ascribed to the precipitation of vernadite and Fe–oxihydroxide from the bottom water layer overlying the sediment within which diagenesis is active. Nodule growth by diagenesis is clearly shown by the mirror relation between compositions of nodules and the underlying sediment. The relation also reflects the latitudinal influence of surface water productivity on the diageneses of nodules and sediment that are more active southward.

ACKNOWLEDGEMENTS

We are very grateful to Drs. J. Hein and M.L. Holmes (U.S. Geological Survey) for their contribution to carry out the Korea–U.S. cooperation research project of manganese nodule study in the Korea Deep Ocean Study (KODOS) area. They have advised a great deal about the scientific design for deep–sea manganese nodule survey. The helps of U.S.G.S. scientists and crew of the R/V Farnella during the cruises are also gratefully acknowledged.

REFERENCES

Aoki, S, Kohyama, N. and Sudo, T., 1979. Mineralogical and chemical properties of smectite in sediment cores from the southeastern Pacific. Deep-Sea Res., 26: 893-902.

Aplin, A. and Cronan, D.S., 1985. Ferromanganese oxide deposits from the central Pacific Ocean. II nodules and associated sediments. Geochim. Cosmochim. Acta, 49: 437-451.

Baker, E.T., Feely, R.A. and Takahashi, K., 1979. Chemical composition, size distribution, and particle morphology of suspended particulate matter at DOMES site A, B, and C: relationships with local sediment composition. In: J.L. Bischoff and D.Z. Piper (Editors), Marine Geology and Oceanography of the Pacific Manganese Nodule Province. Plenum, New York, pp. 163-202.

Bender, M.L., 1971. Does upward diffusion supply the excess manganese in pelagic sediments. J. Geophys. Res., 76: 4212-4215.

Bender, M. L., 1983. The manganese nodule program: EOS., 64(5): 42-43.

Berger, W.H. and Killingley, J.S., 1982. Box cores from the equatorial Pacific: C^{14} sedimentation rates and benthic mixing. Mar. Geol., 45: 93-125.

Berger, W.H., Adeleck, C.G. and Mayer, L.A., 1976. Distribution of carbonate in surface sediments of the Pacific Ocean. J. Geophys. Res., 81(15): 2617-2627.

Berger, W.H., Edkale, A.A. and Bryant, P.P., 1979. Selective preservation of burrows in deep-sea carbonates. Mar. Geol., 32: M205-M230.

Berner, R.A., 1980. Early diagenesis. A theoretical approach. Princeton Univ. Press, New Jersey, 241p.

Bischoff, J.L., Piper, D.Z. and Leong, K., 1981. The alluminosilicate fraction of north Pacific manganese nodules. Geochim. Cosmochim. Acta, 45: 2047-2063.

Bonatti, E., Fisher, D.E., Joensu, O. and Rydell, H.S., 1971. Post-depositional mobility of some transition elements, phosporus, uranium and thorium in deep sea sediments. Geochim. Cosmochim. Acta, 35: 189-201.

Bonatti, E., Kraemer, T. and Rydell, H.S., 1972. Classification and genesis of submarine iron-manganese deposits. In: D.R. Horn (Editor), Ferromanganese Deposits on the Ocean Floor. Nat'l Sci. Found., Washington, pp. 149-166.

Boudreau, B.P. and Scott, M.R., 1978. A model for the diffusion-controlled growth of deep-sea manganese nodules. Am. J. Sci., 248: 903-929.

Burns, R.G. and Burns, V.M., 1975. Mechanisms for nucleation and growth of manganese nodules. Nature, 255(4404): 130-131.

Burns, R.G. and Burns, V.M., 1979. Manganese oxides. In : R.G. Burns (Editor), Marine Minerals. Min. Soc. Am., Short Course Notes 6, Washington, pp. 1-46.

Callender, E. and Bowser, C.J., 1980. Manganese and copper geochemistry of interstitial fluids from manganese nodule rich pelagic sediments of the northeastern equatorial Pacific Ocean. Am. J. Sci., 280: 1063-1096.

Calvert, S.E. and Price, N.B., 1977. Geochemical variation in ferromanganese nodules and associated sediments from the Pacific Ocean. Mar. Chem., 5: 43-74.

Calvert, S.E. and Piper, D.Z., 1984. Geochemistry of ferromanganese nodules from DOMES site A, northern equatorial Pacific: Multiple diagenetic metal sources in the deep sea. Geochim. Cosmochim. Acta, 48: 1913-1928.

Calvert, S.E., Price, N.B., Heath, G.R. and Moore, T.C., Jr., 1978. Relationship between ferromanganese nodule compositions and sedimentation in a small survey area of the equatorial Pacific. J. Mar. Res., 36(1):161-183.

Calvert, S.E., Piper, D.Z. and Baedecker, P.A., 1987. Geochemistry of the rare earth elements in ferromanganese nodules from DOMES A, northern equatorial Pacific. Geochim. Cosmochim. Acta, 51: 2331-2338.

Chester, R., 1990. Marine Geochemistry, Unwin Hyman, London, 698p.

Cole, T.G., 1985. Composition, oxygen isotope geochemistry, and origin of smectite in the metalliferous sediments of the Bauer Deep, southeast Pacific. Geochim. Cosmoshim. Acta, 49: 221-235.

Dymond, J., Lyle, M., Finney, B., Piper, D.Z., Murphy, K., Conard, R. and Pisias, N., 1984. Ferromanganese nodules from MANOP sites H, S, and R. -control of mineralogical and chemical composition by multiple accretionary processes. Geochim. Cosmochim. Acta. 48: 931-950.

Emerson, S., Jahnke, R., Bender, M., Froelich, P., Klinkhammer, G., Browser, C. and Stlock, G., 1980. Early diagenesis in sediments from the eastern equatorial Pacific, I. Porewater nutrient and carbonate results. Earth Planet. Sci. Letts., 49: 963-972.

Emerson, S., Fisher, K., Reimers, C. and Heggie, D., 1985. Organic carbon dynamics and preservation in deep-sea sediments. Deep-Sea Res., 32: 1-21.

Finney, B., Heath, G.R. and Lyle, M., 1984. Growth rates of ferromanganese nodules at MANOP site H (easternnorth Pacific). Geochim. Cosmochim. Acta, 48: 911–920.

Fisher, K., 1984. Particle fluxes to the eastern tropical Pacific Ocean– sources and processes. Corvallis, Oregon State Univ., Ph.D. Thesis, 225p.

Forstner, U. and Stoffers, P., 1981. Chemical fractionation of transition elements in Pacific pelagic sediments. Geochim. Cosmochim. Acta, 45: 1141–1146.

Friedrich, G., Pluger, W.L. and Kunzendorf, H., 1988. Chemical composition and of manganese nodules. In: P. Halbach, P. Friedrich, and U. von Stackelberg (Editors), The Manganese Nodule Belt ofthe Pacific Ocean. Geological environment, nodule formation, and mining aspects. Ferdinand Enke Verlag Stuttgart, pp. 37–51.

Giovanoli, R. and Arrhenius, G., 1988. Structural chemistry of marine manganese and synthetic model. In: P. Halbach, P. Friedrich, and U. von Stackelberg (Editors), The Manganese Nodule Belt ofthe Pacific Ocean. Geological environment, nodule formation, and mining aspects. Ferdinand Enke Verlag Stuttgart, pp. 20–37.

Glasby, G.P., Stoffers, P., Sioulas, A., Thijssen, T. and Friedrich, G., 1982. Manganese nodule formation in the Pacific Ocean: a general theory. Geo–Mar. Letts., 2: 47–53.

Graybeal, A.L. and Heath, G.R., 1984. Remobilization of transition metals in surficial pelagic sediments from the eastern Pacific. Geochim. Cosmochim. Acta, 48: 965–976.

Greenslate, J.L., Fisk, M.B. and Felix, D., 1979. Systematics in manganese concretion composition in the northeastern equatorial Pacific. In: C. Lalou (Editor). La Genese des Nodules de Manganese. Proc. Colloq. Int. CNRS, No. 289, pp. 39–54.

Halbach, P. and Ozkara, M., 1979. Morphological and geochemical classification of deep–sea ferromanganese nodules and its genetic interpretation. In: C. Lalou (Editor). La Genese des Nodules de Manganese. Proc. Colloq. Int. CNRS, No. 289: pp. 77–88.

Halbach, P., Scherhag, C., Hebisch, U. and Marchig, V., 1981. Geochemical and mineralogical control of different genetic types of deep–sea nodules from the Pacific Ocean. Mineral Deposita. 16: 59–84.

Halbach, P., Giovanoli, R. and von Borstel, D., 1982. Geochemical processes controlling the relationship between Co, Mn and Fe in early diagenetic deep–sea nodules. Earth Planet. Sci. Letts., 60: 226–236.

Halbach, P., Friedrich, P. and von Stackelberg, U., 1988. The manganese nodule belt of the Pacific Ocean. Geological environment, nodule formation, and mining aspects. Ferdinand Enke Verlag Stuttgart, 254p.

Hartmann, M. and Muller, P.J., 1982. Trace metals in interstitial waters from central Pacific Ocean sediments. In: K.A. Fanning, and F.T. Manheim (Editors), The dynamic environment of the ocean floor. Lexington Books, Lexington, pp.285–301.

Hein, J.R., Yeh, H.W. and Alexander, E., 1979. Origin of iron–rich montmorillonite from the manganese nodule belt of the north equatorial Pacific. Clays and Clay Minerals, 27: 185–194.

Hein J.R., Swab, W.C. and Davis, A.S., 1988. Cobalt– and platinum–rich ferromanganese crusts and associated substrate rocks from the Marshall Islands. Mar. Geol., 78: 255–283.

Heye, D. and Marchig, V., 1977. Relationship between growth rate of manganese nodules from the central Pacific and their chemical constitution. Mar. Geol., 23: M19–M25.

Heye, D., Marchig, V. and Meyer, H., 1979. The growth of buried manganese nodules. Deep–Sea Res., 26A: 789–798.

Horn, D.R., Horn, B.M. and Delach, M.N., 1973. Copper and Nickel content of ocean ferromanganese deposits and their relation to properties of the substrate. In: M. Morgenstein (Editor), The Origin and Distribution of Manganese Nodules in the Pacific and Prospects for Exploration. Valdivia Manganese Exploration Group, Univ. of Hawaii and IDOE/NSF, Honolulu, pp. 71–76.

Huh, C.A. and Ku, T.L., 1984. Radiochemical observations on manganese nodules from three sedimentary environments in the north Pacific. Geochim. Cosmochim. Acta, 48: 951–963.

Jahnke, R., Heggie, D., Emerson, S. and Grundmanis, V., 1982. Pore waters of the central Pcaific Ocean: nurient results. Earth. Planet. Sci. Letts., 61: 233–256.

Johnson, T.C., 1976. Biogenic opal presevation in pelagic sediments of a small area in the eastern tropical Pacific. Geol. Soc. Am Bull., 87: 1273–1282.

Kalhorn, S. and Emerson, S., 1984. The oxidation state of manganese in surface sediments of the deep sea. Geochim. Cosmochim. Acta, 48: 897–902.

Klinkhammer, G.P., 1980. Early diagenesis in sediments from the equatorial Pacific, II. Porewater results. Earth and Planet. Sci. Letts., 49: 81–101.

Klinkhammer, G.P., Heggie, D. and Graham, D., 1982. Metal diagenesis in

oxidative marine sediments. Earth Planet. Sci. Letts., 61: 211–219.

Krishnaswami, S., 1976. Authigenic transition elements in Pacific pelagic clay. Geochim. Cosmochim. Acta, 40: 425–434.

Krishnaswami, S. and Cochran, J.K., 1978. Uranium and thorium series nuclides in oriented ferromanganese nodules : growth rates, turnover times and nuclide behaviour. Earth Planet. Sci. Letts., 40: 45–62.

Ku, T.L. and Broecker, W.S., 1969. Radiochemical studies on manganese nodules from deep–sea origin. Deep–Sea Res., 16: 625–637.

Lallier–Verges, E. and Alberic, P., 1989. Burrowing: a major process in the Mn–Ni enrichment of red clays. Mar. Geol., 86: 75–79.

Lalou, C., Bricht, E., Poupeau, G., Romary, P. and Jehanno, C., 1979. Growth rates and possible age of a north Pacific nodule. In: J.L. Bischoff and D.Z. Piper (Editors), Marine Geology and Oceanography of the Pacific Manganese Nodule Province. Plenum, New York, pp 815–834.

Li, Y.H., 1982. Interelement relationship in abyssal Pacific ferro– manganese nodules and associated pelagic sediments. Geochim. Cosmochim. Acta., 46: 1053–1060.

Lyle, M., 1982. Estimating growth rates of ferromanganese nodules from chemical compositions: implications for nodule formation processes. Geochim. Cosmochim. Acta, 46: 2301–2306.

Lyle, M., 1983. The brown–green color transition in marine sediments: a marker of the Fe(III)–Fe(III) redox boundary. Limnol. Oceanogr., 28: 1026–1033.

Lyle, M., Heath, G.R. and James, M.R., 1984. Transport and release of transition elements during early diagenesis : Sequential leaching of sediments from MANOP sites M and H. Part I. pH 5 acetic acid leach. Geochim. Cosmochim. Acta, 48: 1705–1715.

Lyle, M., Murray, D.W., Finney, B.P., Dymond, J., Robbins, J.M. and Brooksforce, K., 1988. The record of late Pleistocene biogenic sedimentation in the eastern tropical Pacific Ocean. Paleocenogr., 3: 39–59.

Lynn, D.C. and Bonatti, E., 1965. Mobility of manganese in diagenesis of deep–sea sediments. Mar. Geol., 3: 457–474.

Macdougall, J.D., 1979. The distribution of total alpha radioactivity in selsected manganese nodules from the North Pacific: implications for growth processes. In: J.L. Bischoff and D.Z. Piper (Editors), Marine Geology and Oceanography of the Pacific Manganese Nodule Province. Plenum New

York, pp. 775–789.

Marchig, V. and Gundlach, H., 1979. Diagenetic changes in the radiolarian oozes of the central Pacific and their influence on the growth of manganese nodules. In: C. Lalou (Editor), La Genese des Nodules de Manganese. Colloq. Int. CNRS., No. 289: 55–60.

Marchig, V. and Gundlach, H., 1981. Separation of iron from manganese and growth of manganese nodules as a consequence of diagenetic ageing of radiolarians. Mar. Geol., 40: M35–M43.

Margolis, S.V. and Glasby, G.P., 1973. Microlaminations in marine manganese nodules as revealed by scanning microscopy. Geol. Soc. Am. Bull., 84: 3601–3610.

Martin, J.H. and Knauer, G.A., 1984. VERTEX: manganese transport with $CaCO_3$. Deep–Sea Res., 30(4A): 411–425.

McKelvey, V.E., Wright, N.A, and Rowland, R.W., 1979. Manganese nodule resources in the northeastern equatorial Pacific. In: J.L. Bischoff and D.Z. Piper (Editors), Marine Geology and Oceanography of the Pacific Manganese Nodule Province. Plenum, New York, pp 747–762.

Moorby, S.A. and Cronan, D.S., 1981. The distribution of elements between co–existing phases in some marine ferromanganese oxide deposits. Geochim. Cosmochim. Acta, 45: 1855–1877

Moore, W.S., 1984. Thorium and radium isotopic relationships in manganese nodules and sediments at MANOP site S. Geochim. Cosmochim. Acta, 48: 987–992.

Moore, W.S., Ku, T.L., Macdougall, J.D., Burns, V.M., Burns, R., Dymond, J., Lyle, M. and Piper, D.Z., 1981. Fluxes of metals to manganese nodule: radiochemical, chemical, structural, and mineralogical studies. Earth Planet. Sci. Letts., 52: 151–171.

Muller, J.P. and Mangini, A., 1980. Organic carbon decomposition rates in sediments of the Pacific manganese nodule belt dated by ^{230}Th and ^{231}Pa. Earth Planet. Sci. Letts., 51: 94–114.

Munsell, 1988. Soil color chart. MacBeth Div., Kolmorgen Corp., Mayland.

Murray, J.W., Balistrieri, L.S. and Paul, B., 1984. The average oxidation states of manganese in marine sediments and ferromanganese nodules. Geochim. Cosmochim. Acta, 48: 1237–1248.

Normark, W.R. and Spiess, F.N., 1976. Erosion on the Line Islands archepelgic apron: effect of small scale topographic relief. Geol. Soc. Am. Bull., 87:286–296.

Paul, A.Z., Thorndike, E.M., Sullivan, L.G., Heezen, B.C. and Gerard, R.D., 1978. Observation of the deep-sea floor from 202 days of time-lapse photography. Nature. 272: 812-814.

Piper, D.Z., 1988. The metal oxide fraction of pelagic sediment in the equatorial north Pacific Ocean: a source of metals in ferro- manganese nodules. Geochim. Cosmochim. Acta, 52: 2127-2145.

Piper, D.Z. and Williamson, M.E, 1977, Composition of Pacific Ocean ferromanganese nodules. Mar. Geol., 23: M285-M303.

Piper, D.Z. and Blueford, J.R., 1982. Distribution, mineralogy, and texture of manganese nodules and their relation to sedimentation at DOMES site A in the equatorial north Pacific. Deep-Sea Res., 29(8A): 927-952.

Piper, D.Z., Basler, J.R. and Bischoff, J.L., 1984. Oxidation state of marine manganese nodules. Geochim. Cosmochim. Acta, 48: 2347-2355.

Piper, D.Z., Rude, P.D. and Monteith, S., 1987. The chemistry and mineralogy of haloed burrows in pelagic sediment at DOMES Site A : the equatorial North Pacific. Mar. Geol., 74: 41-55.

Prahl, F.G., Muehlhausen, L.A. and Lyle, M., 1989. An organic geochemical assessment of oceanographic conditions at MANOP site C over the past 26,000 years. Paleocenogr., 4(5): 495-510.

Quinterno, P. and Theyer, F., 1979. Biostratigraphy of the equatorial north Pacific DOMES sites A, B, and C. In: J.L. Bischoff and D.Z. Piper (Editors), Marine Geology and Oceanography of the Pacific Manganese Nodule Province. Plenum, New York, pp. 349-364.

Qunby-Hunt, M.S. and Turekian, K.K., 1983, Distribution of elements in seawater. EOS, 64: 130-131.

Raab, W.J., 1972. Physical and chemical features of Pacific deep sea manganese nodules and their implication to genesis of nodules. In: D.R. Horn (Editor), Ferromanganese Deposits on the Seafloor. NSF, Washington. pp. 31-49.

Reyess, J.L., Marchig, V. and Ku, T.L., 1982. Rapid growth of a deep-sea manganese nodule. Nature, 295: 401-403.

Reyess, J.L., Lemaitre, N., Ku, T.L., Marchig, V., Southon, J.R., Nelson, D.E. and Vogel, J.S., 1985. Growth of a manganese nodule from Peru Basin: a radiochemical anatomy. Geochim. Cosmochim. Acta, 49: 2401-2408.

Sawlan, J.J. and Murray, J.W., 1983. Trace metal remobilization in the interstitial waters of red clay and hemipelagic sediments. Earth Planet. Sci. Letts., 64: 213-230.

Schink, D.R. and Guinasso, N.L. Jr., 1977. Redistribution of dissolved and adsorbed materials in abyssal marine sediments undergoing biological manganese nodule belt dated by ^{230}–Th and ^{231}Pa. Earth Planet. Sci. Letts., 51: 94–114.

Segl, M., Mangini, A., Beer, J., Bonani, G., Suter, M. and Wolfli, W., 1989. Growth rate variations of manganese nodules and crusts induced by paleoceanographic events. Paleocenogr., 4(5): 511–530.

Skornyakova, N.S., 1979. Zonal regularities in occurrence, morphology, and density of manganese nodules of the Pacific Ocean. In: J.L. Bischoff and D.Z. Piper (Editors), Marine Geology and Oceanography of the Pacific Manganese Nodule Province. Plenum, New York, pp. 699–727.

Skornyakova, N.S. and Zaikin, V.N., 1988. Local variability of iron–manganese nodules in the eastern Clarion–Clipperton ore province. Oceanology, 28 (4): 487–491.

Skornyakova, N.S. and Murdmaa, I.O., 1992. Local variations in distribution and composition of ferromanganese nodules in the Clarion–Clipperton nodule province. Mar. Geol., 103: 381–405.

Smith, K.L. and Baldwin, R.J., 1984. Seasonal fluctuations in deep–sea sediment community oxygen consumption : central and eastern north Pacific. Nature, 307: 624–626.

Sorem, R.K., 1973. Manganese nodules as indicators of long–term variations in seafloor environment. In: M. Morgenstein(Editor), Papers on the on Origin and Distribution of Manganese Nodules in the Pacific and Prospects for Exploration. Valdivia Manganese Exploration Group, Univ. of Hawaii and IDOE/NSF, Honolulu, pp 151–164.

Sorem, R. K. and Fewkes, R.H., 1979. Manganese Nodules, Research Data and Methods of Investigation. Plenum, New York, 723p.

Stoffers, P., Sioulas, A., Glasby, G.P. and Thijssen, T., 1982. Geochemical and sedimentological studies of a box core from the western sector of the Peru Basin. Mar. Geol., 49: 225–240.

Takematsu, N., Kusakabe, H., Sato, Y. and Okabe, S., 1988. Todorkite formation in seawater by microbial mediation. J. Oceanogr. Soc. Japan, 44:235–243.

Thiel, H. and Schneider, J., 1988. Manganese nodule–organism interactions. In: P. Halbach, G. Friedrich and U. von Stackelberg (Editors), The Manganese Nodule Belt of the Pacific Ocean. Geological environment, nodule formation, and mining aspects. Ferdinand Enke, Stuttgart, pp. 102–110.

Turner, S. and Buseck, P.R., 1981. Todorokite ; a new family of naturally occurring manganese oxides. Science, 212: 456–458.

Usui, A., 1979. Nickel and copper accumulation as essential elements in 10 A ° manganite of deep–sea manganese nodules. Nature, 279: 411–413.

van Andel, T.H., Heath, G.R. and Moore T.C. Jr., 1975. Cenozoic history and paleocenography of the central equatorial Pacific Ocean. Geol. Soc. Am. Mem., 143: 1–134p.

Welton, J.E., 1984, SEM petrology atlas, Am. Assoc. Petrol. Geologists, Tulsa, Oklahoma, 237p.

Wendt, J., 1974, Encrusting organisms in deep–sea manganese nodules. In:K.J. Hsu and H.C. Jenkyns (Editors), Pelgic Sediments: on Land and Under the Sea. IAS Spec. Publ., No. 1, pp. 437–447.

Wolfart, R., 1988. Radiolarian biostratigraphy of the Cenozoic. In: P. Halbach, G. Friedrich and U. von Stackelberg (Editors), The Manganese Nodule Belt of the Pacific Ocean. Geological environment, nodule formation, and mining aspects. Ferdinand Enke, Stuttgart, pp. 115–126

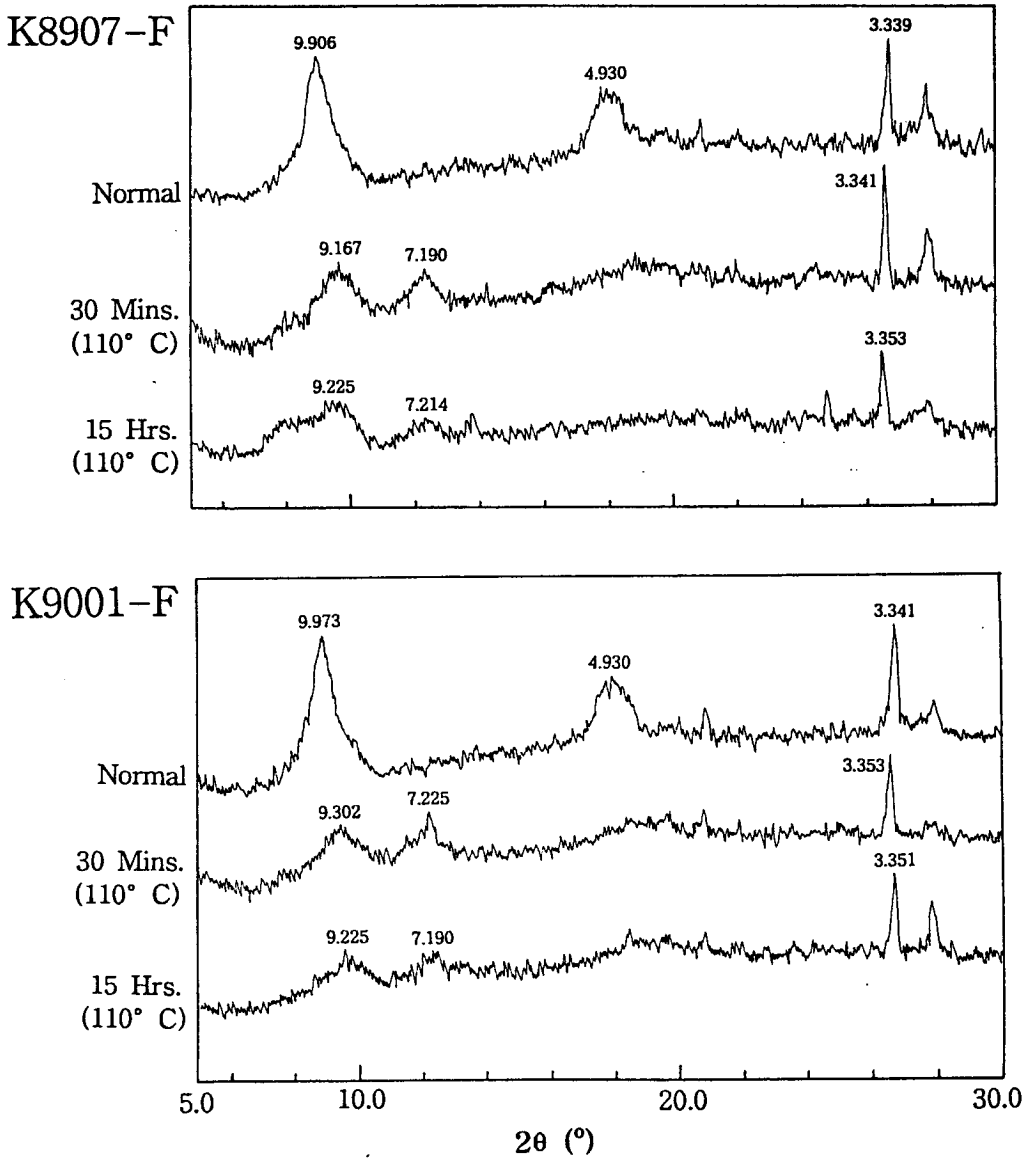

Fig. 2. X-ray diffraction pattern of Mn-nodule powder showing distinct decrease of 10 Å and occurrence of 7 Å peaks by dehydration at 110 ℃ for 30 minutes and 15 hours. It reveals 10 Å-manganate that consists of both todorokite and buserite.

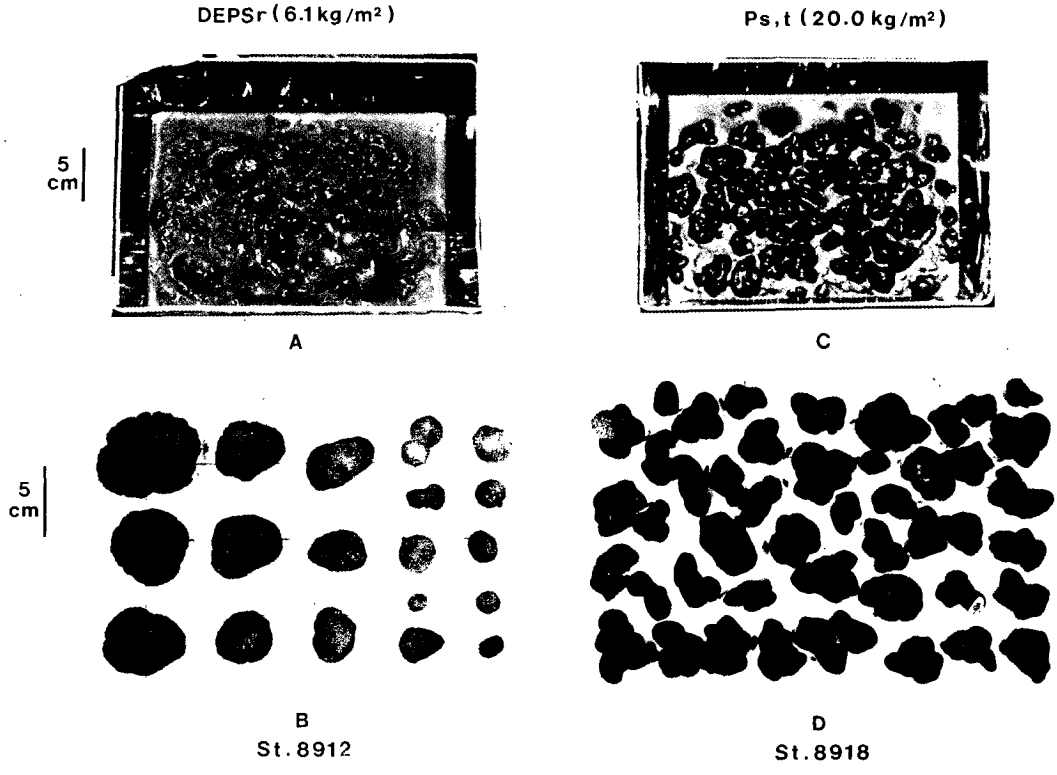

Fig. 3. Occurrence of nodule types in box cores. R-type nodules are mostly mononucleated and occur partially or embedded within the topmost sediment layer (A and B). S- and T-type nodules are polynucleated and exposed on sediment surface (C and D).

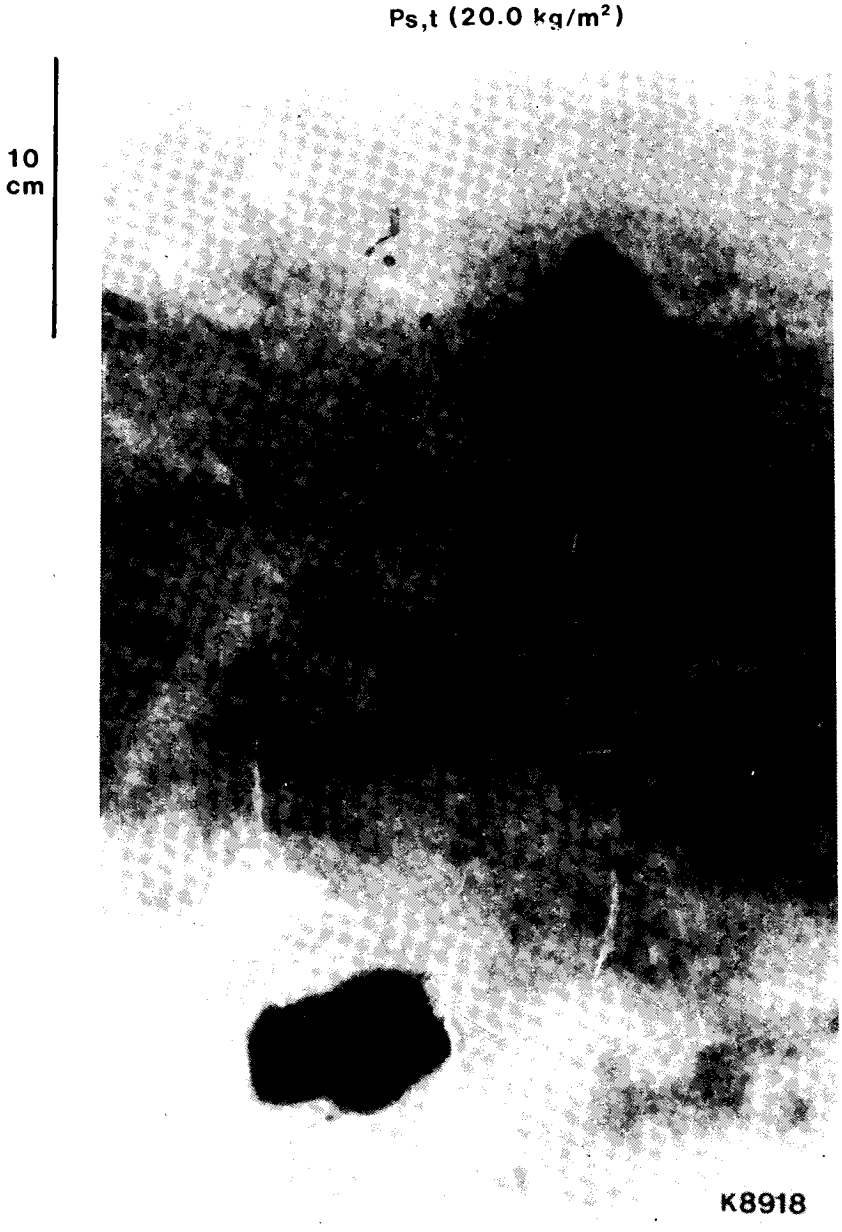

Fig. 4. X-radiograph showing buried nodules (st. 8918). A polynucleated nodule in the upper part shows smooth surface top within unit 1 and rough bottom within unit 2. In the lowermost unit 3, the nodule is rimmed with loose outermost layer of Mn-oxide grains. On the seafloor, polynucleated S- and T-type nodules are abundant (20.0 kg/m^2).

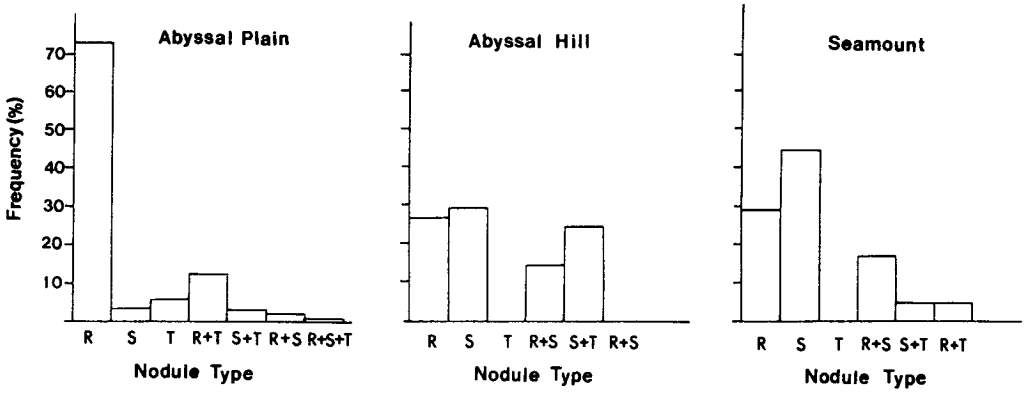

Fig. 5. Occurrence of nodule types (in frequency %) and its relation to seafloor morpholgy. R-type nodules are dominant in abyssal plain, whereas S-types are abundant in hill and seamount areas. T-types occur with either R- or S-type nodules.

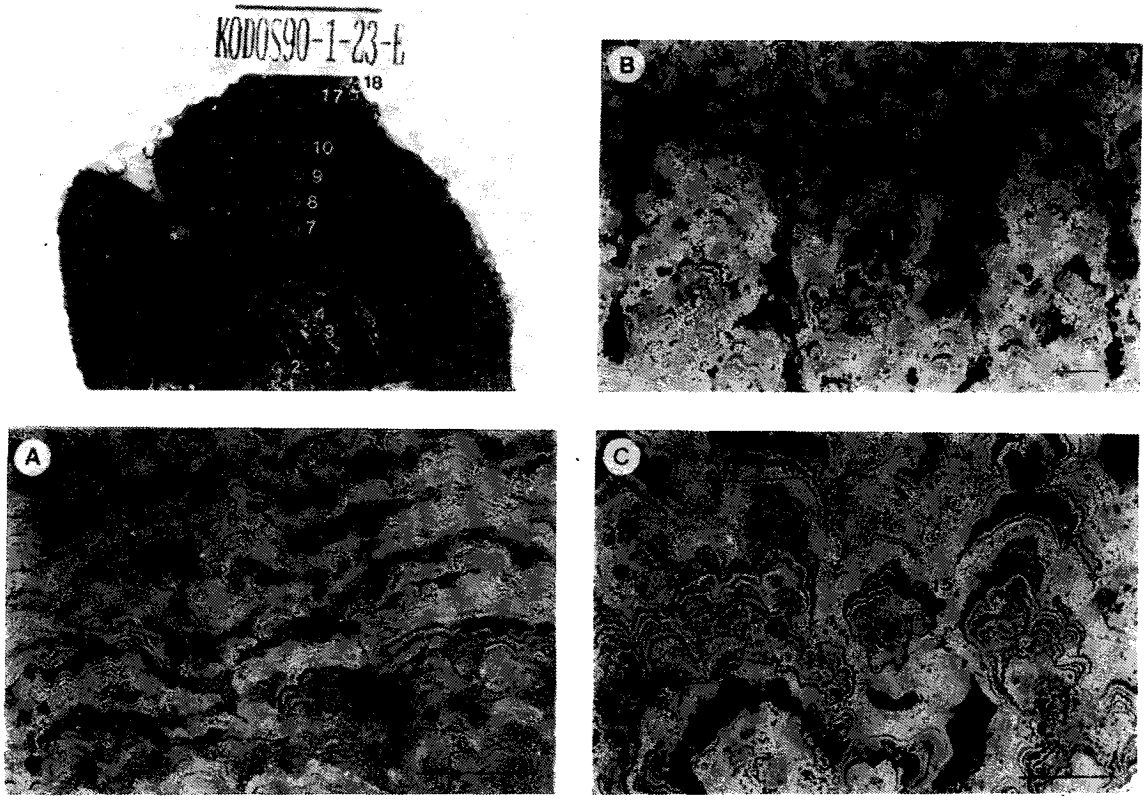

Fig. 6. Internal structures and distribution of metal species in selected nodules. Structures were photographed (bar: 1 cm) and examined in detail using electron back-scattered microphotograph (bar : 100 μm). Todorokite (buserite) is grayish to white, whereas vernadite is dark gray to dark in color. Concentration of metals is presented by histogram at points with open circles and numbers. Todorokite (buserite), vernadite, and non-nodular materials are respectively presented by white, black, and hatched bars. 1) Structures of R-type nodule. Todorokite (buserite) layers are discontinuous and irregular, intercalated with sedimentary clasts (A). Todorokite (buserite) generally forms botryoids (B), massive, dendritic and cauliflower-like structures (C).

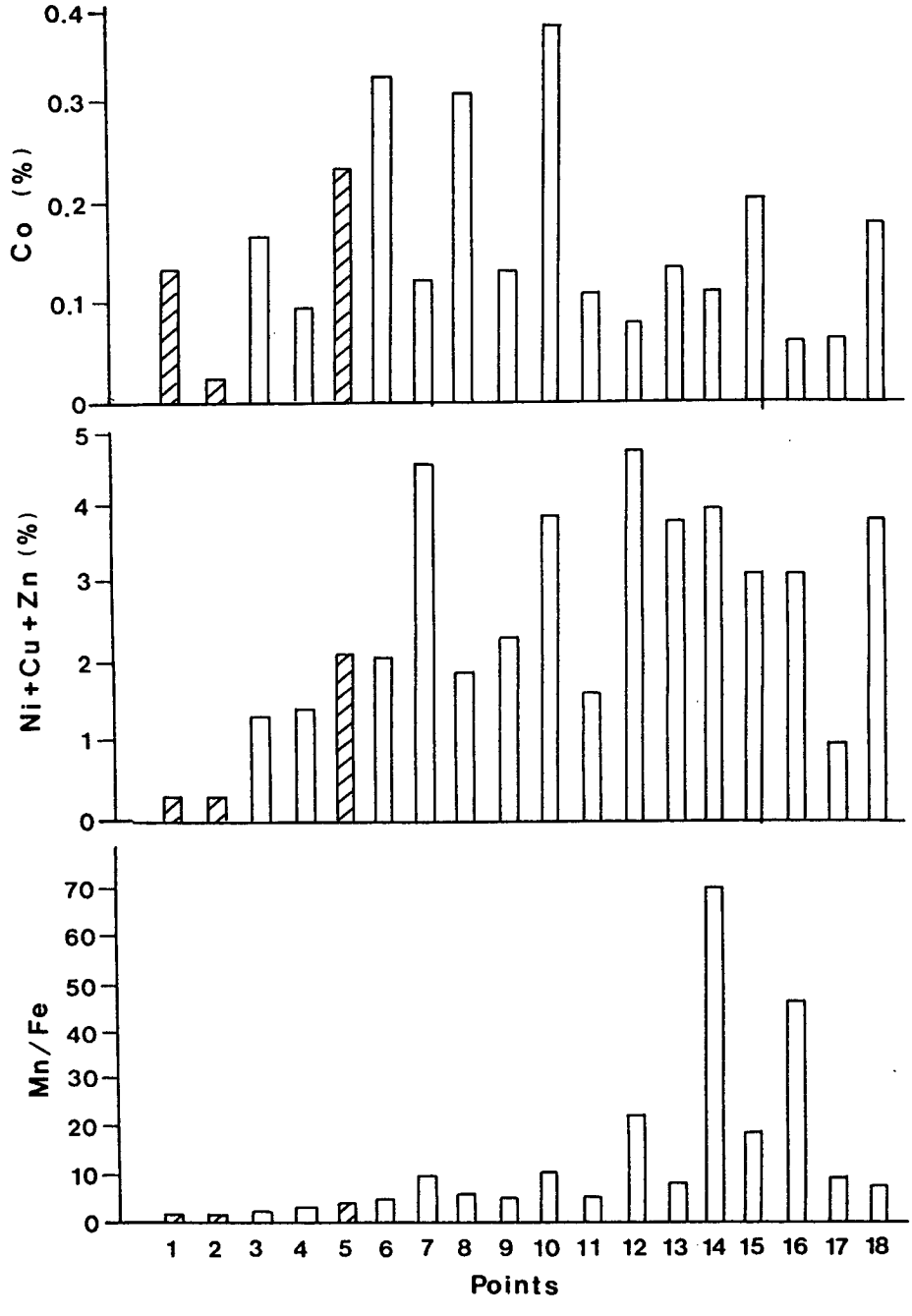

Fig. 6–1D. Distribution of metal species (Co, Ni+Cu+Zn) and Mn/Fe ratio at points of internal structures.

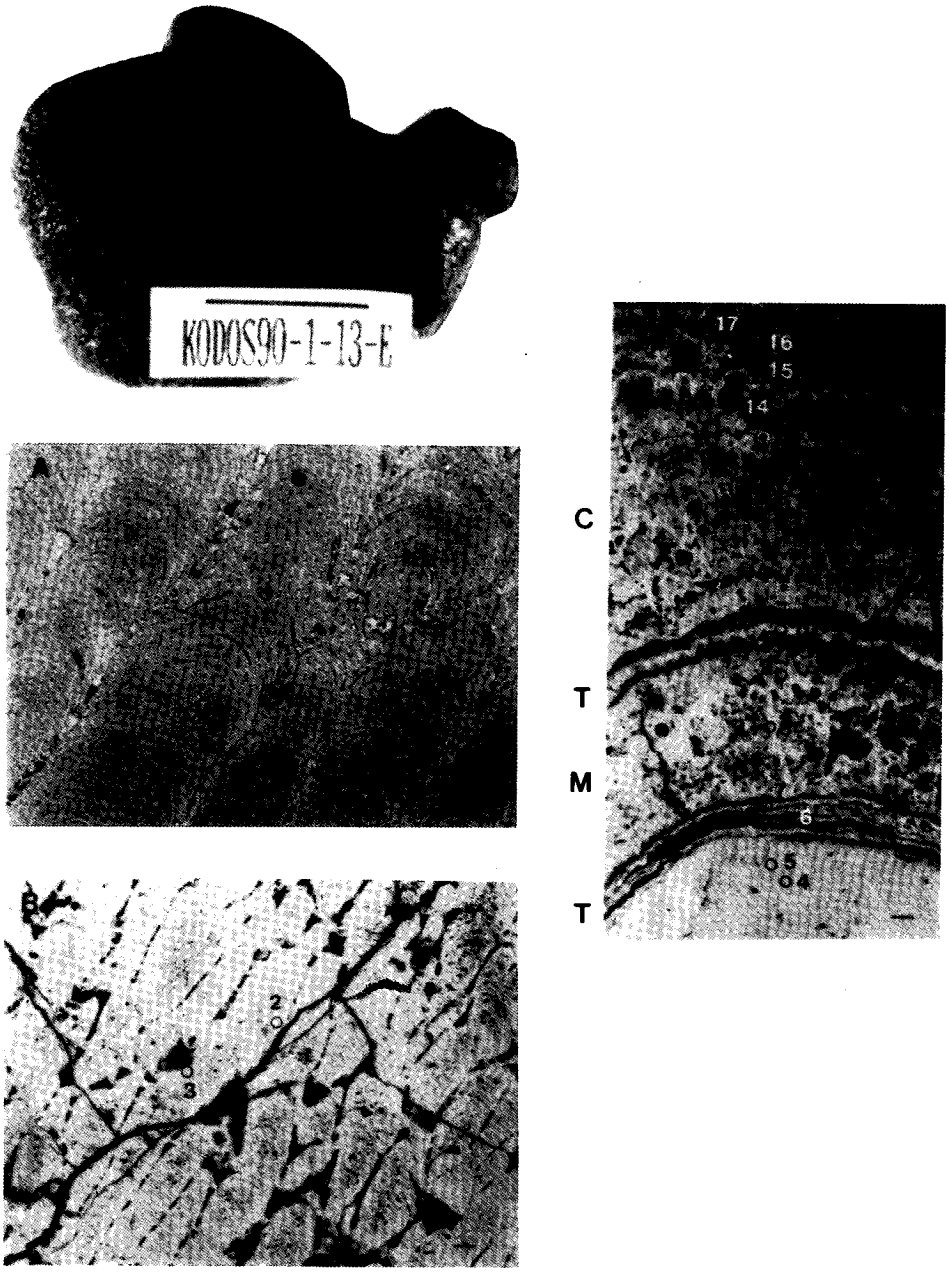

Fig. 6–2. S–type nodule showing distinct change in structures. Nuclei comprise old S–type nodule or Mn–crusts with typical columnar structures of vernadite (A and B). Growth patterns change outward (C) from the core, thin laminations of todorokite (buserite) and vernadite (T), massive structures of todorokite (buserite) (M), T, to columnar zone of vernadite (C).

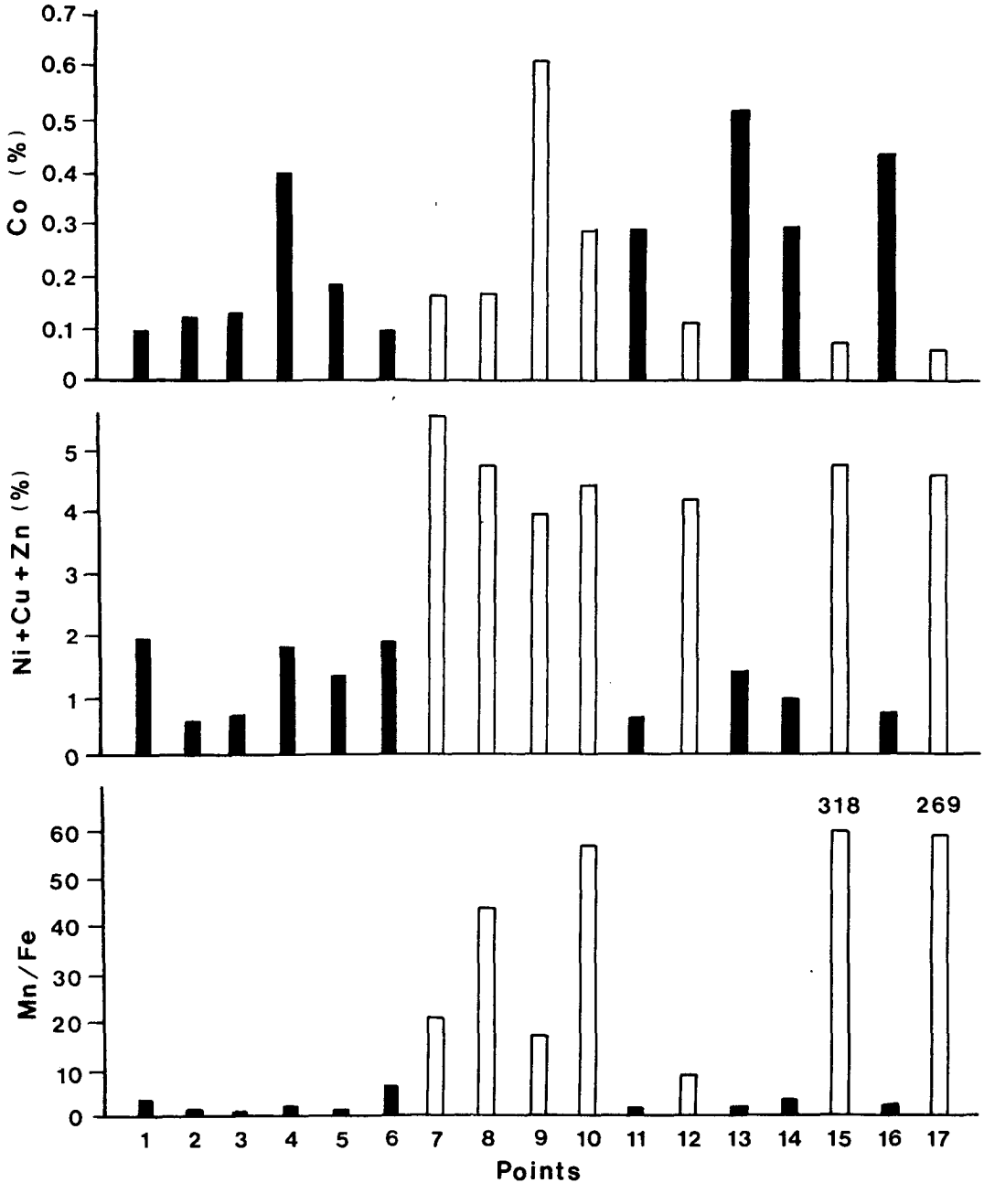

Fig. 6-2D. Distribution of metal species (Co, Ni+Cu+Zn) and Mn/Fe ratio at points of internal structures.

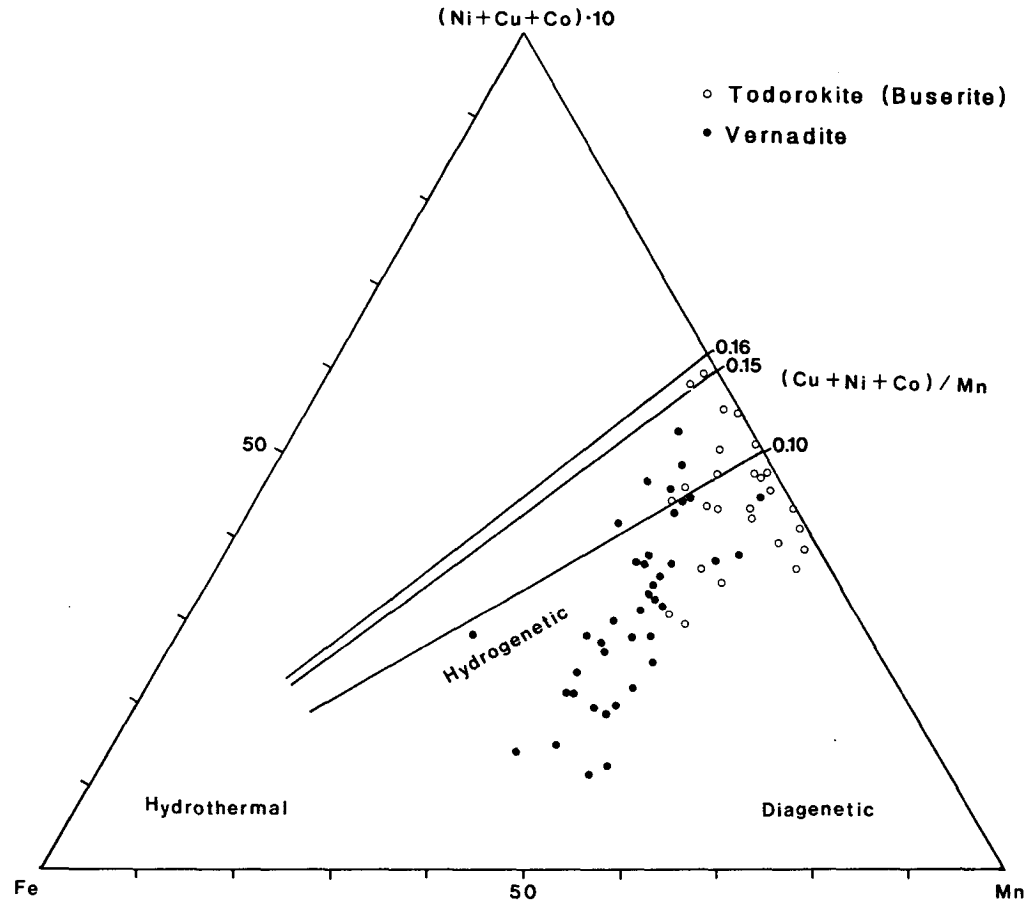

Fig. 7. Ternary relationship of Mn, Fe, and 10(Ni+Cu+Co) in mineral species (after Usui, 197b). It shows that todorokite (buserite) is of diagenetic and vernadite is of hydrogenetic origin. Open circle represents todorokite (buserite); filled one, vernadite.

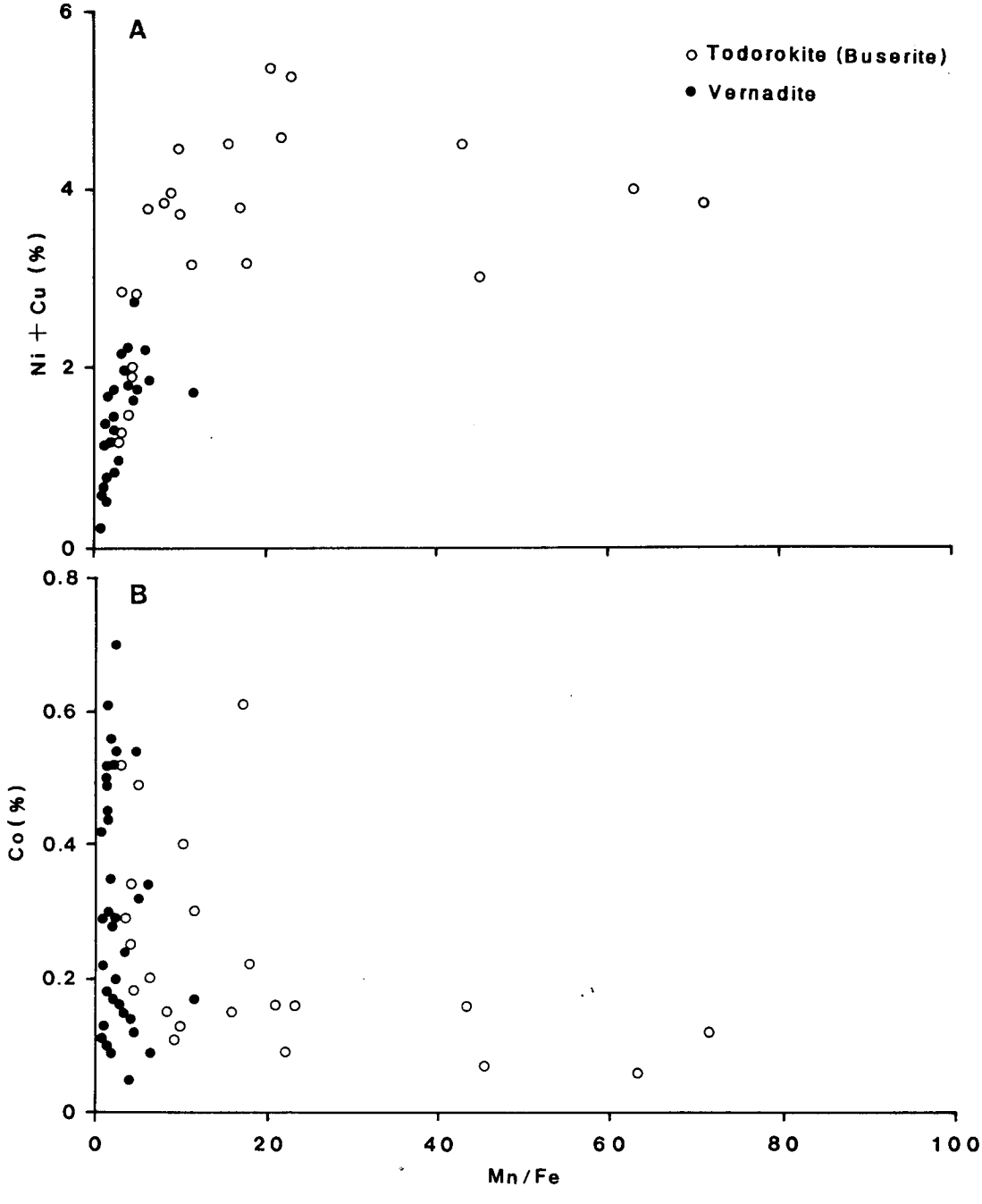

Fig. 8. Relations of Ni+Cu (A) and Co to Mn/Fe ratio (B) in mineral species. (For symbols, see Fig. 7).

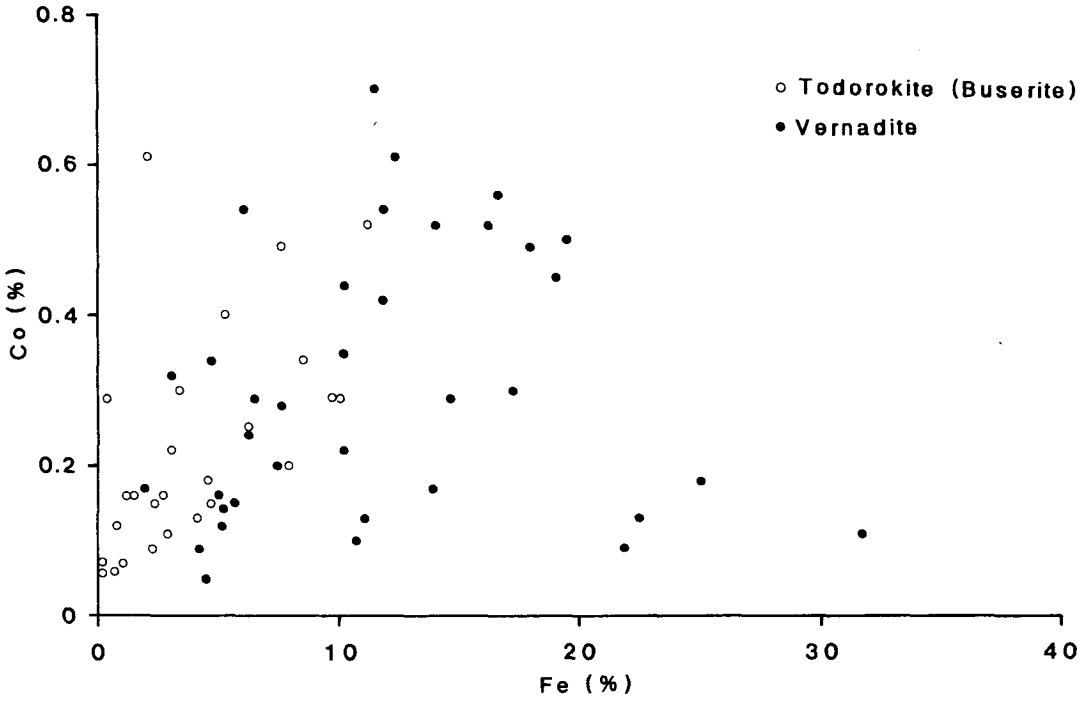

Fig. 9. Relation of Co to Fe in mineral species.

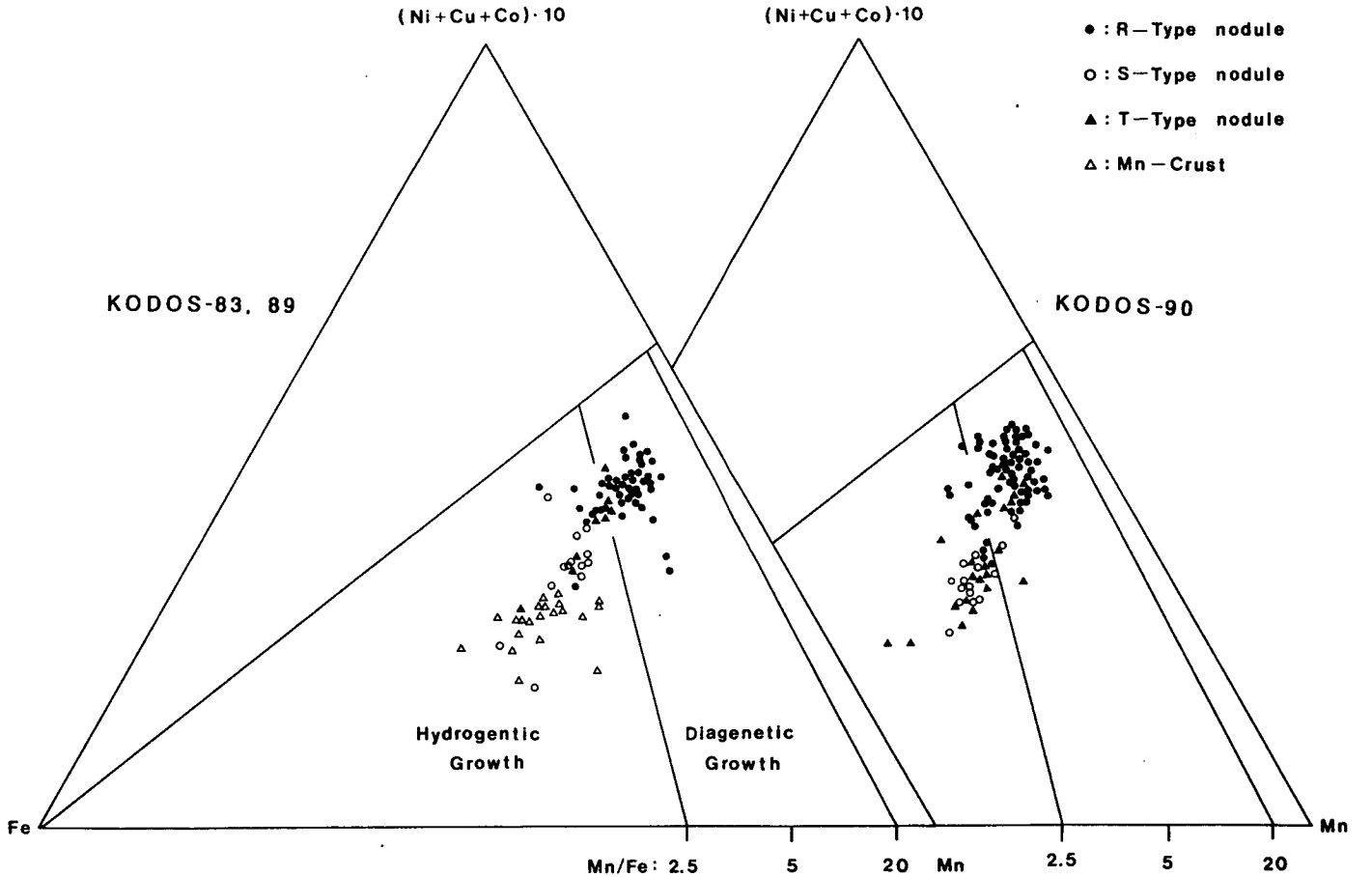

Fig. 10. Ternary relationships of Mn, Fe, and 10 (Ni+Cu+Co) showing distinct genetic divisions of nodule types (Bonatti et al., 1972). Mn-crusts from the Marshall Islands are also plotted for comparison. Open and filled circles represent S- and R-type nodules; open and filled triangles, Mn-crusts and T-type nodules, respectively.

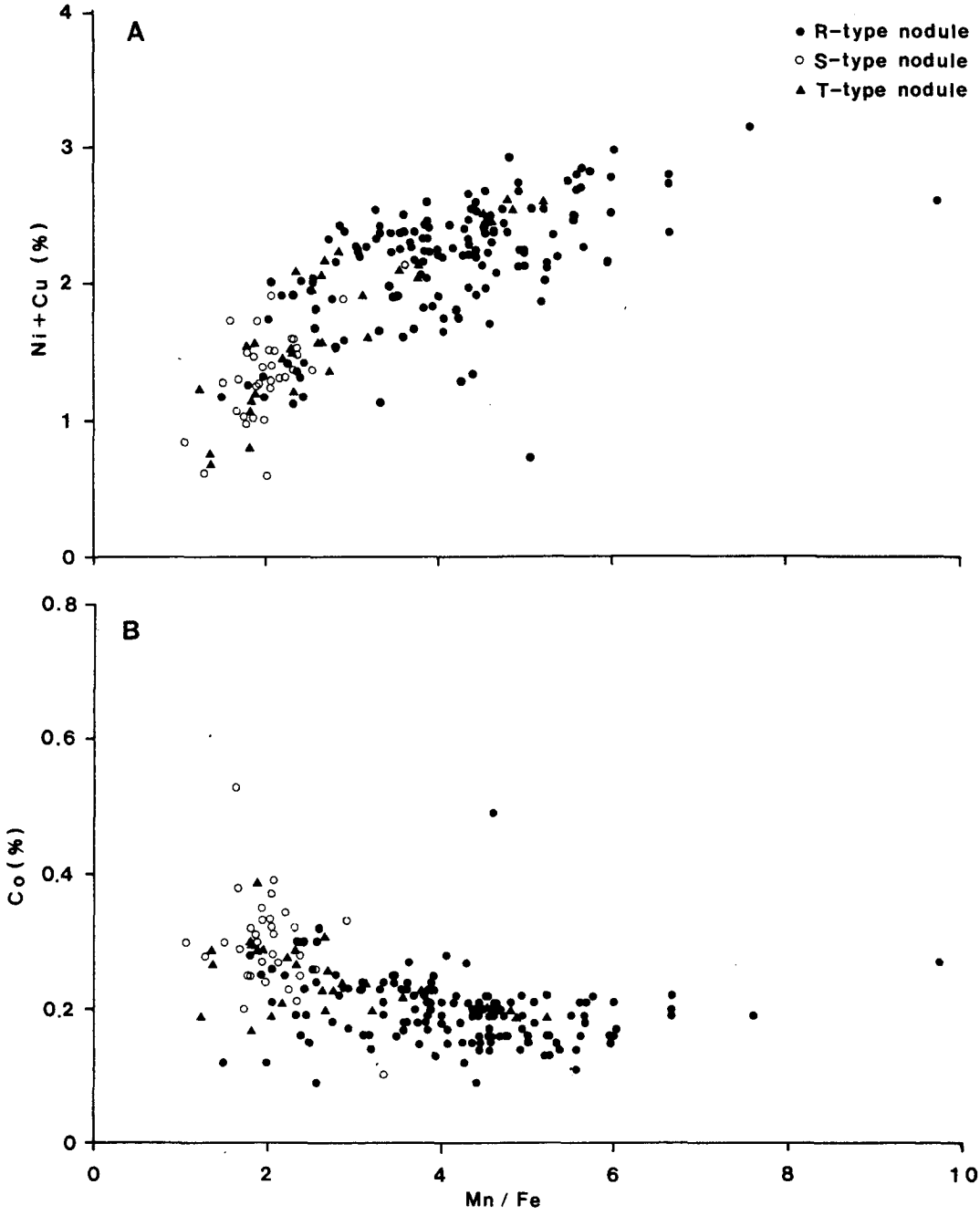

Fig. 11. Relations of Ni+Cu (A) and Co to Mn/Fe ratio (B) in nodules. (For symbols, see Fig. 10).

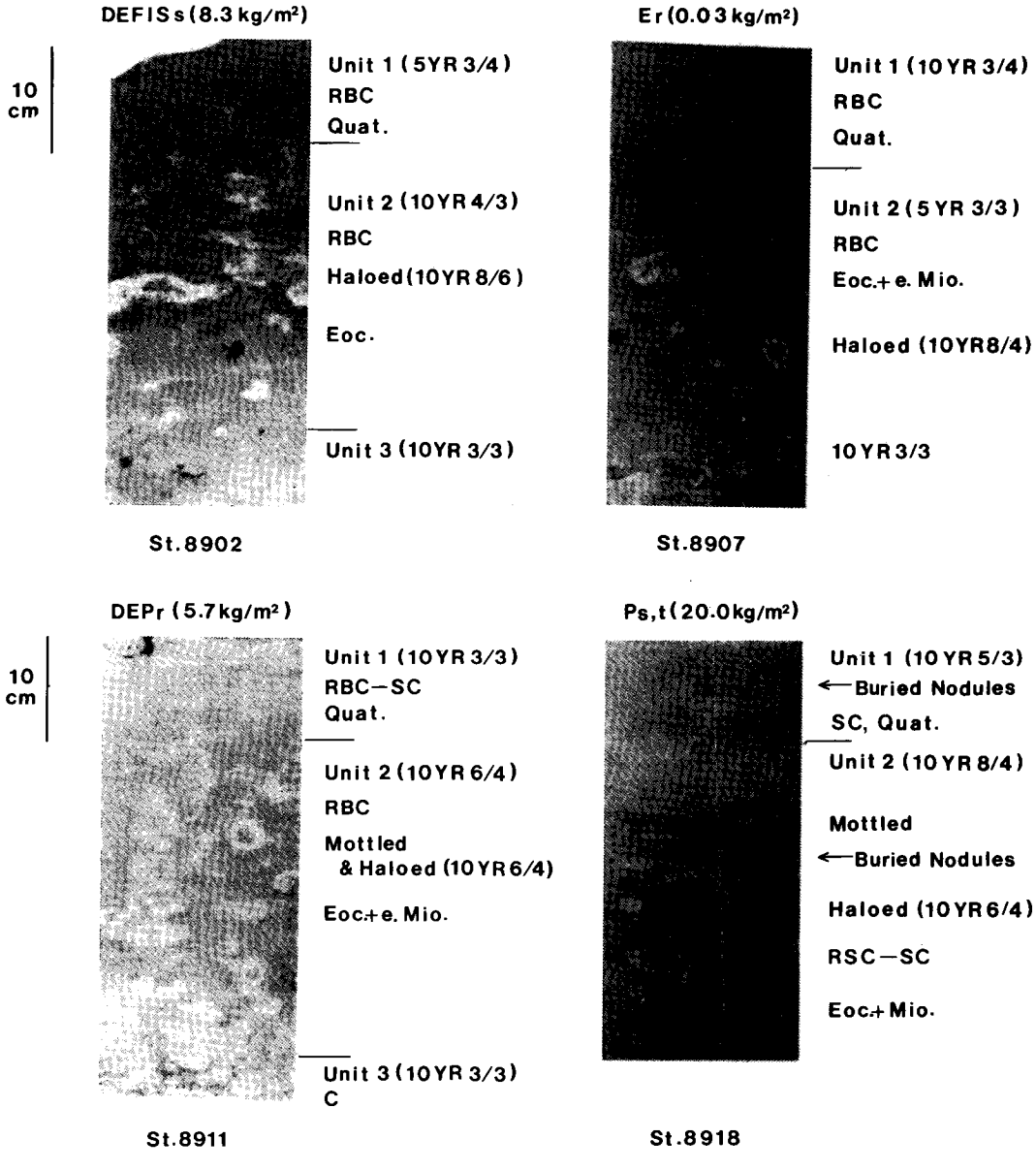

Fig. 12. General characters of box core sediments. The sediments are divided into 2 to 3 units, based on color, lithology, bioturbation, and ages. Unit 1 is assigned to the late Quaternary, and the lower units, Tertiary (Pliocene to Eoceone) by radiolarian fossils. Topmost bold letters are shapes of associated nodules. D is discoidal; E, ellipsoidal; F, flaty; I, irregular; S, spheroidal; P, polynucleated in shape. Subscript : r is rough; s, smooth; t, transitional in surface texture. RBC. radiolarian-bearing clay; SC, siliceous clay; CNO, calcareous nannofossil ooze; SO, siliceous ooze.

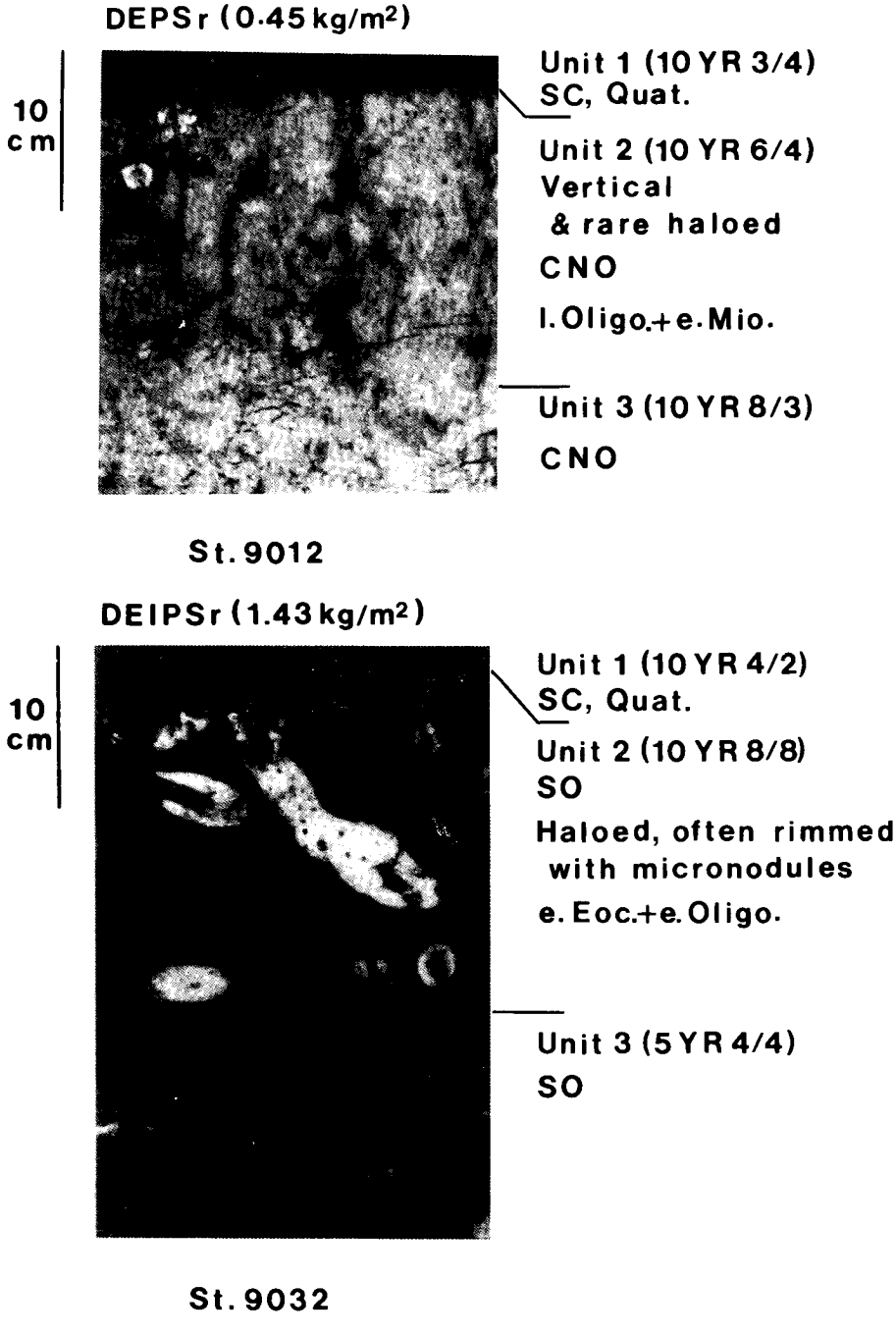

Fig. 12. (continued)

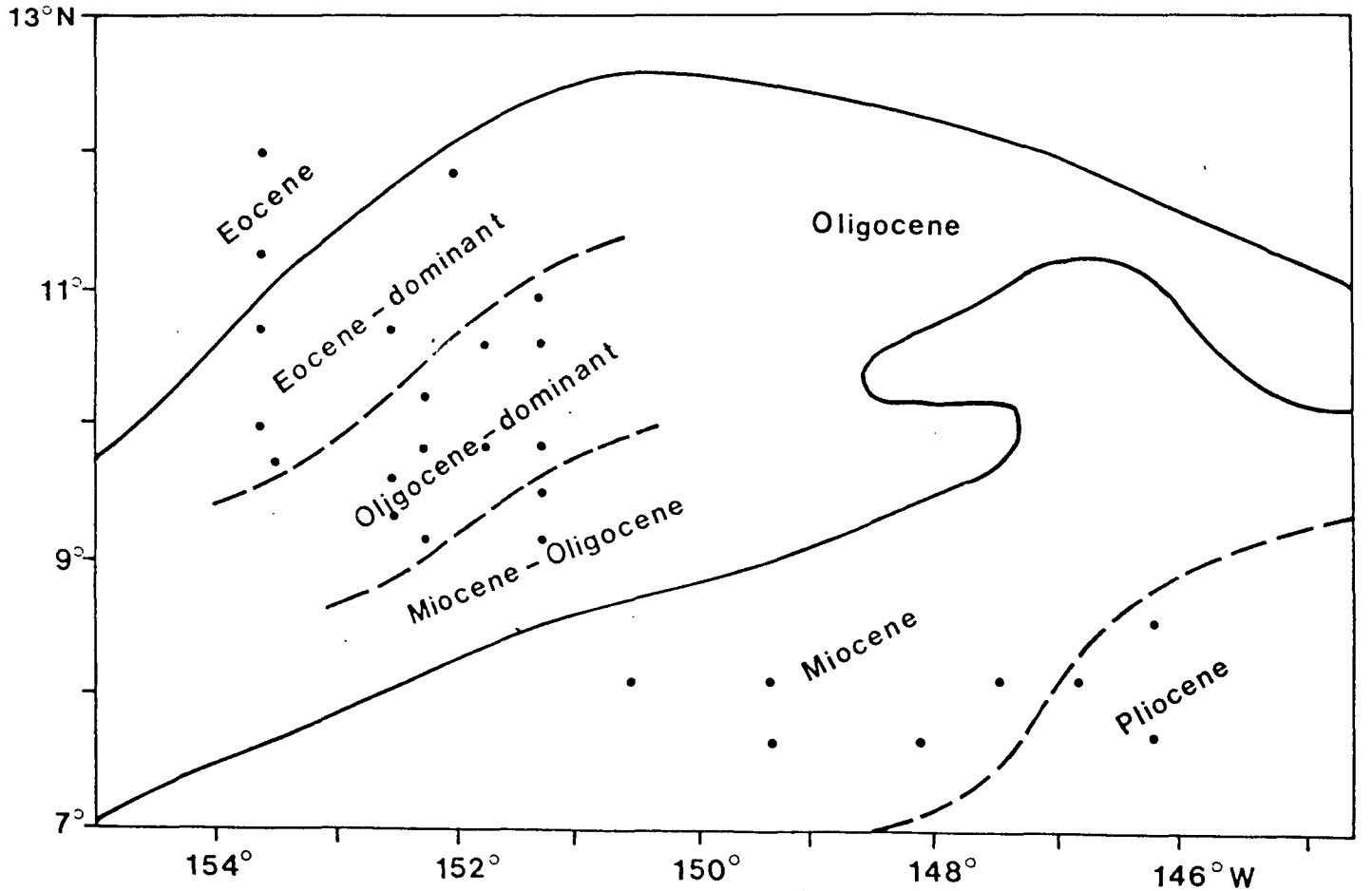

Fig. 13. Age distribution of Tertiary radiolarian fossils in unit 1, combined with the datings of 26 box cores (dashed lines) and the general distribution (thick lines) in the northeast equatorial Pacific (Ryan and Heezen, 1978).

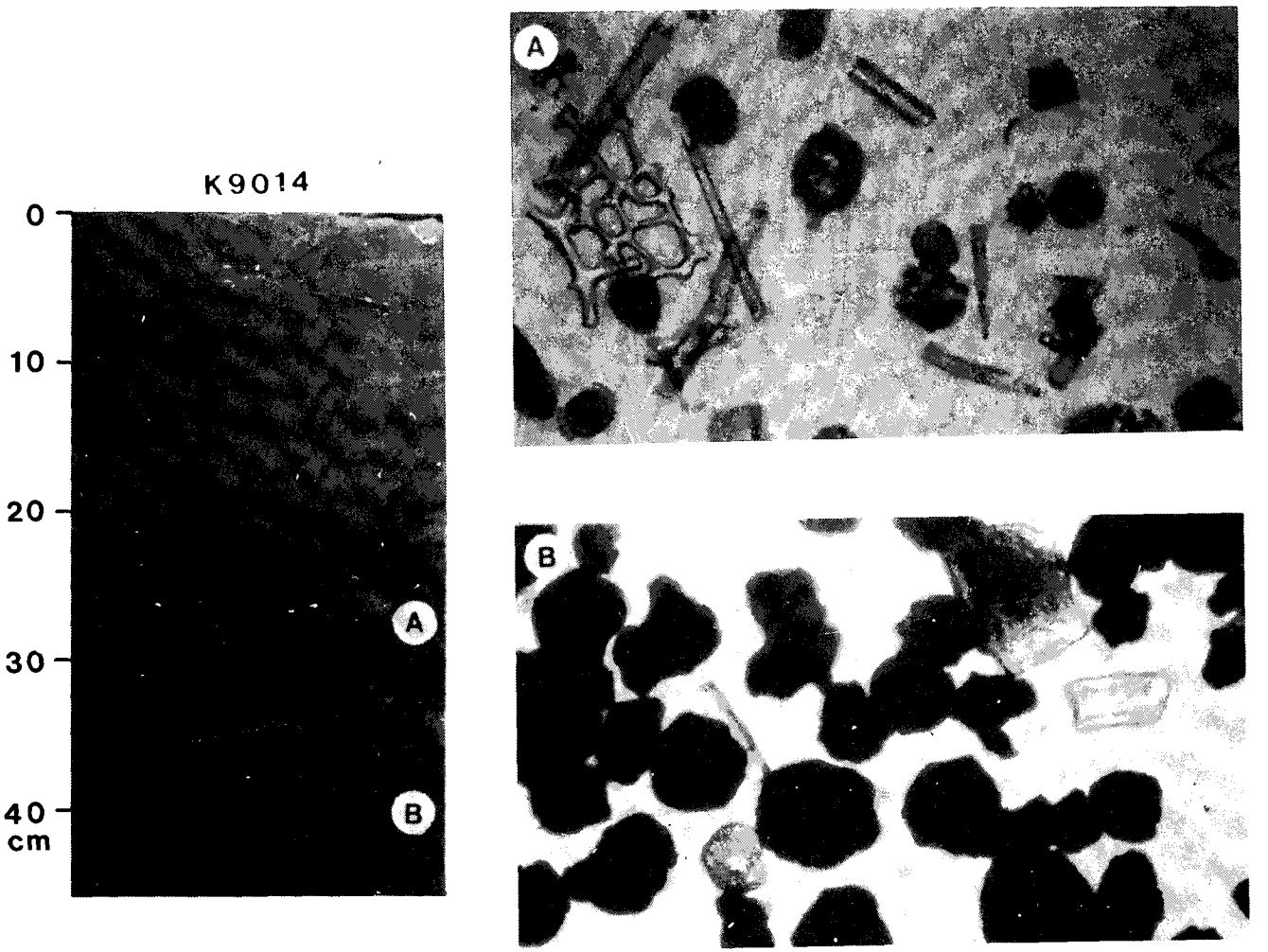

Fig. 14. Coarse (>62 μm) particles (60 folds in magnification) in core no. K9014. In units 1 and 2, they consist mainly of resistant radiolarian fossil fragments. The lowermost unit 3 is characterized by large amounts of micronodule often with smectite grains.

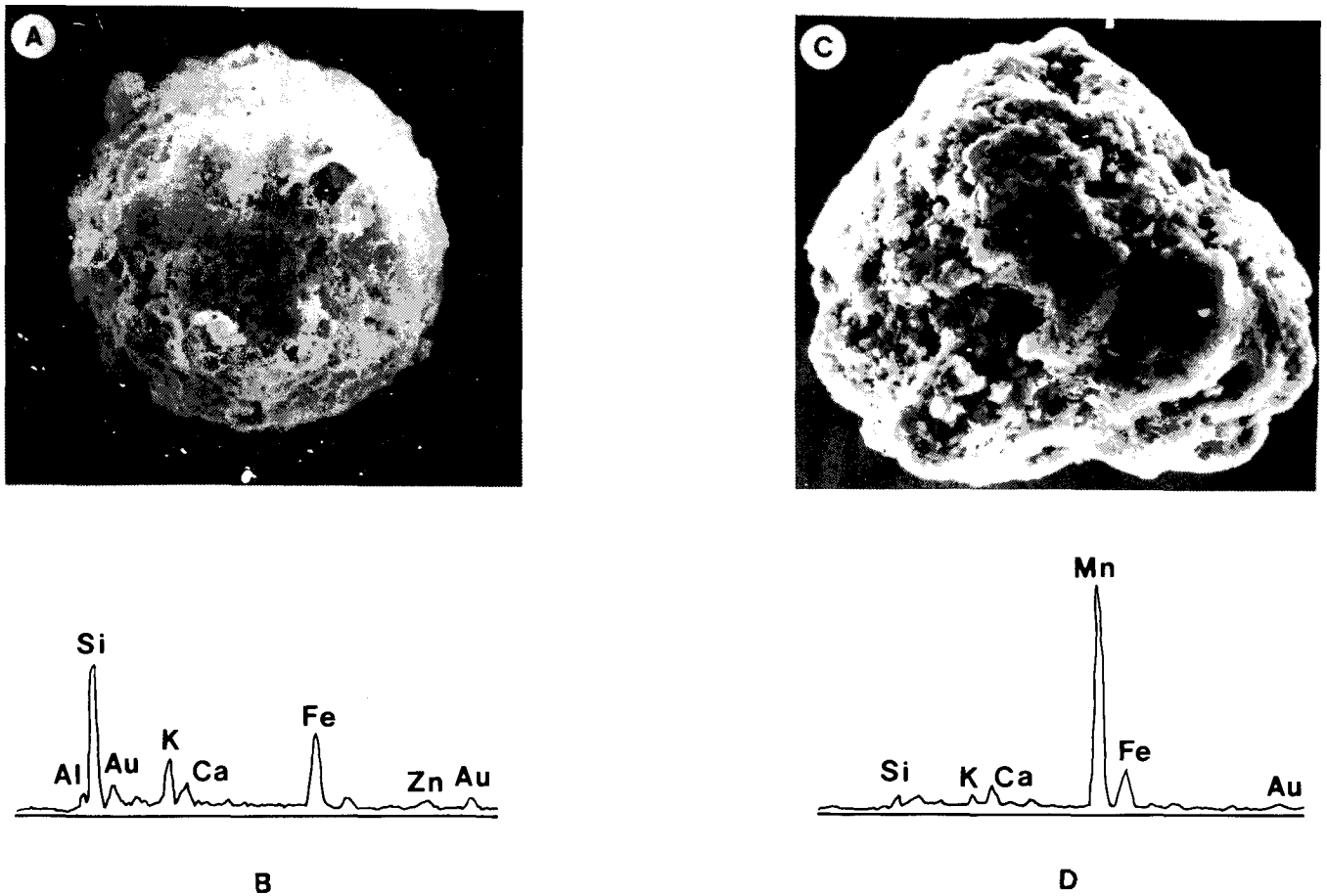

Fig. 15. SEM photographs and EDX spectra of smectite (A and B) and micronodule (C and D), which were picked in >63 μm size fraction at 40 cm depth of K9037 core.

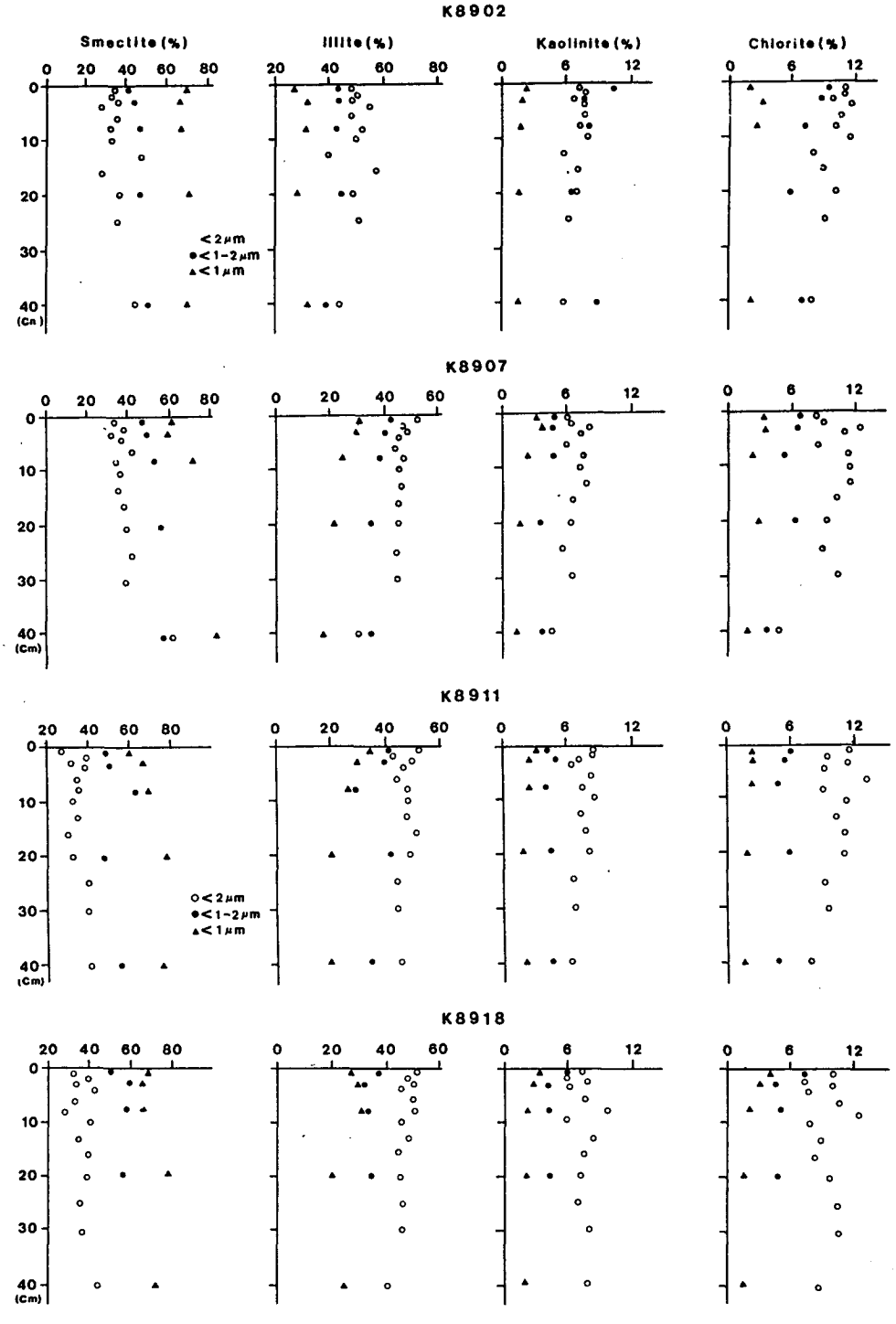

Fig. 16. Distribution of clay minerals in selective cores (nos., K8902, K8907, K8911, and K8918). Filled circles represent smectite; open circles, illite, triangles, sum of kaolinite and chlorite.

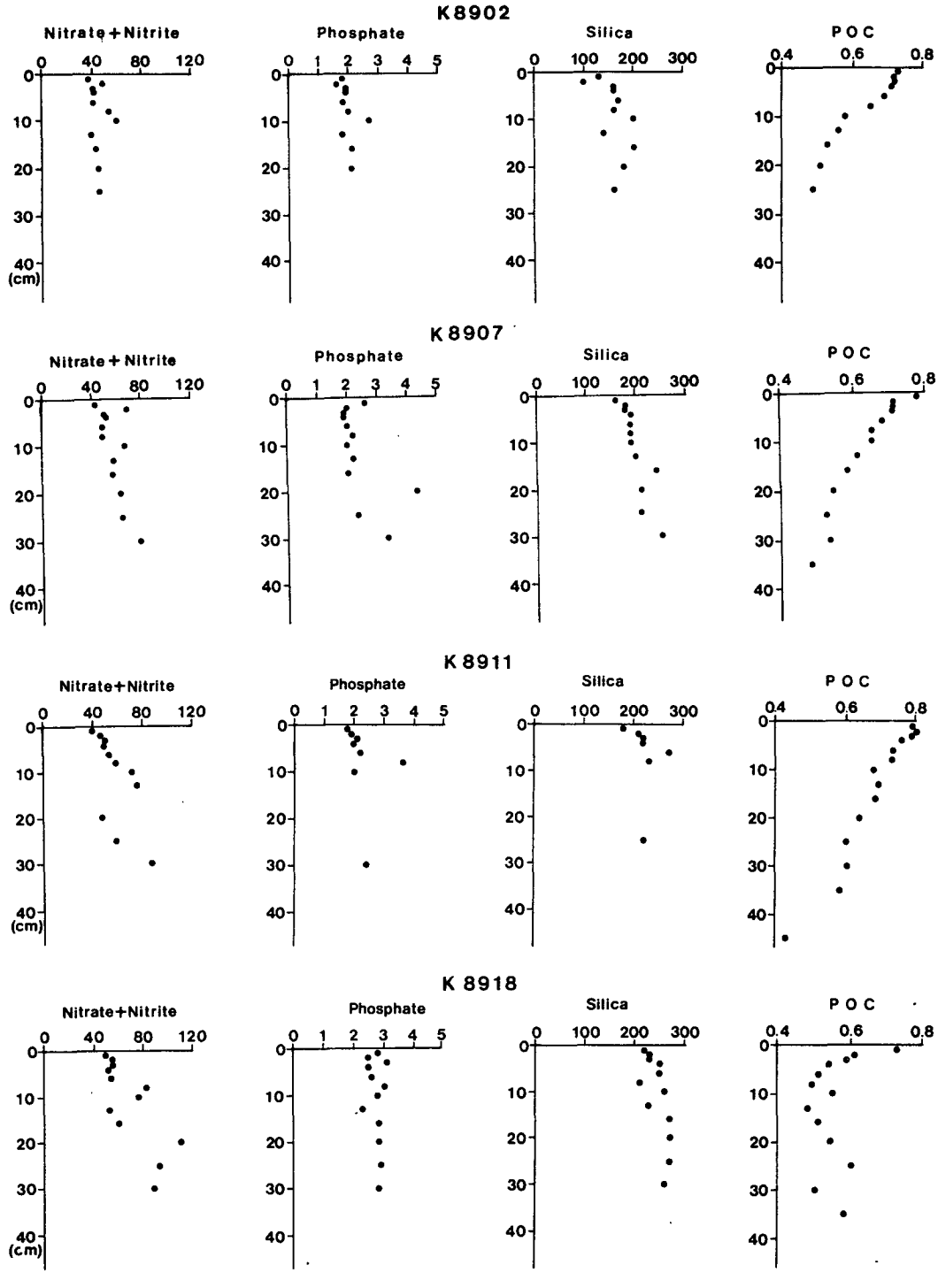

Fig. 17. Distirbution of porewater nutrients (nitrate+nitrite, phosphate, and silica) and particulate organic carbon (POC, %) in selected box cores (nos., K8902, K8907, K8911, and K8918).

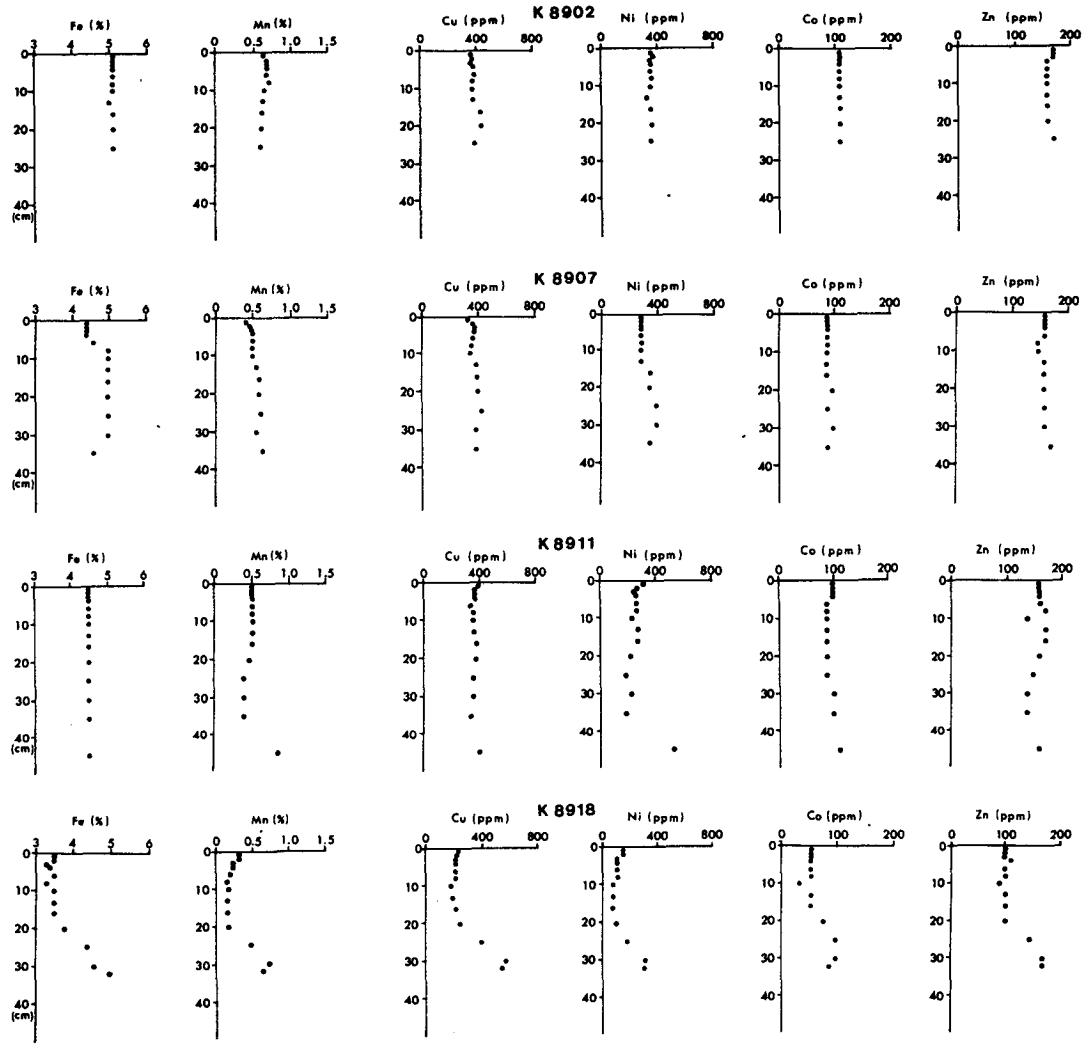

Fig. 18. Distirbution of metal species in selected box core (nos., K8902, K8907, K8911, and K8918) sediment. Fe and Mn are presented in %; Ni, Cu, Co, and Zn in ppm.

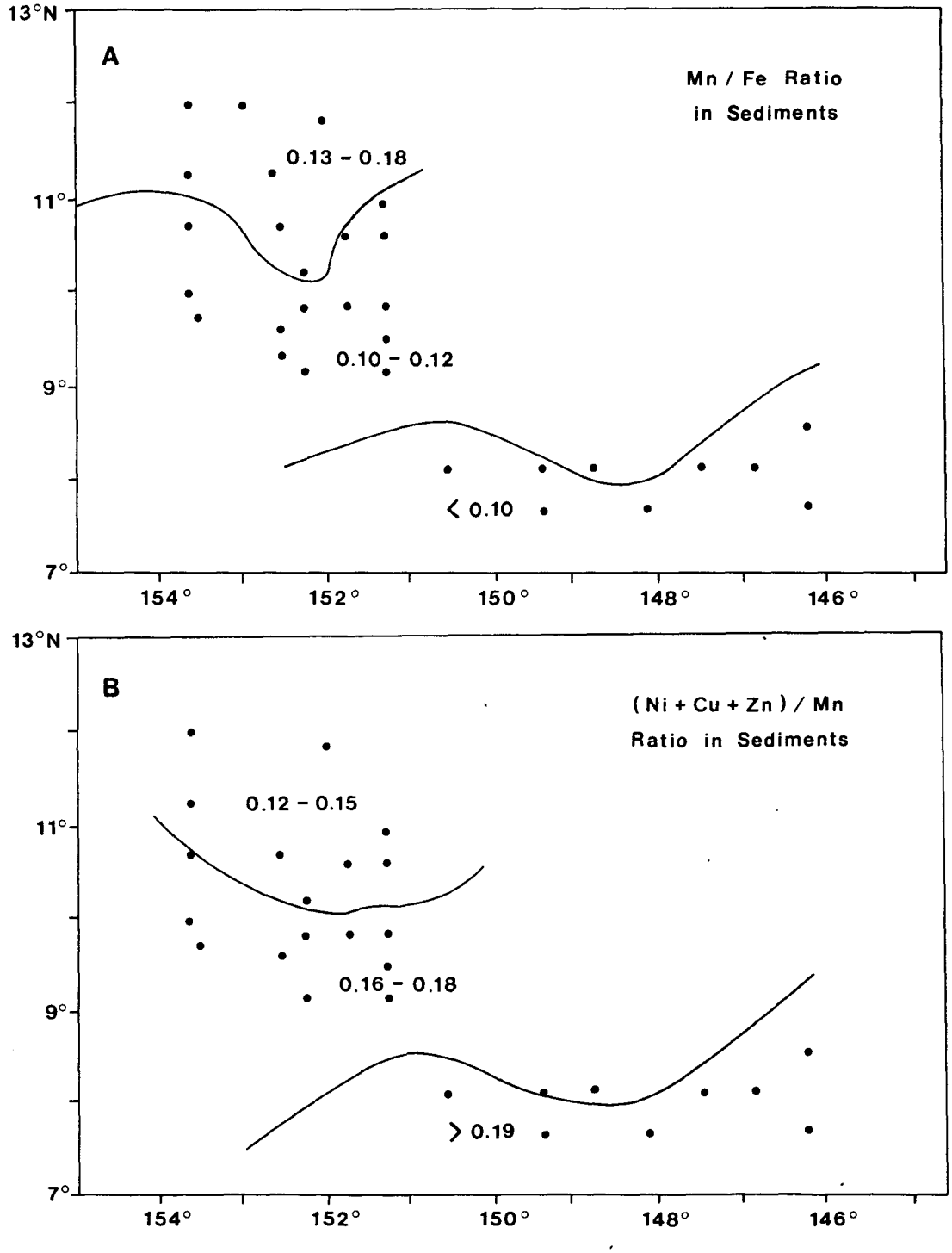

Fig. 19. Regioanl distribution of averge Mn/Fe (A) and Ni+Cu+Zn/Mn ratios (B) in the topmost sediment unit 1.

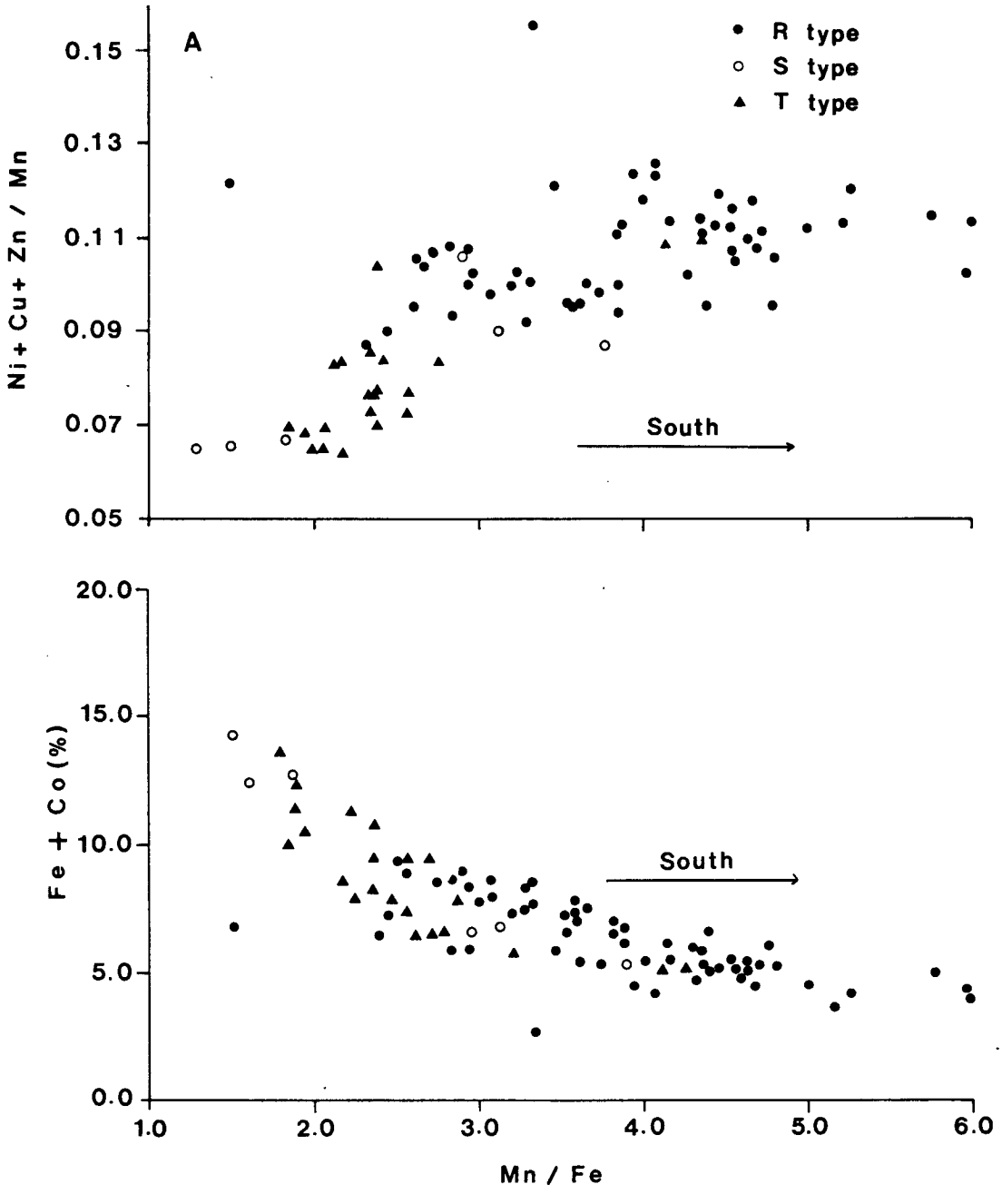

Fig. 20. Relation of Ni+Cu+Zn/Mn and Fe+Co to Mn/Fe ratio in nodules (A), and Ni+Cu+Zn/Mn to Mn/Fe ratio in units 1, 2, and 3 of the underlying sediment (B). The data were selected in box core sediment containing nodules. (For symbols, see Fig. 7).

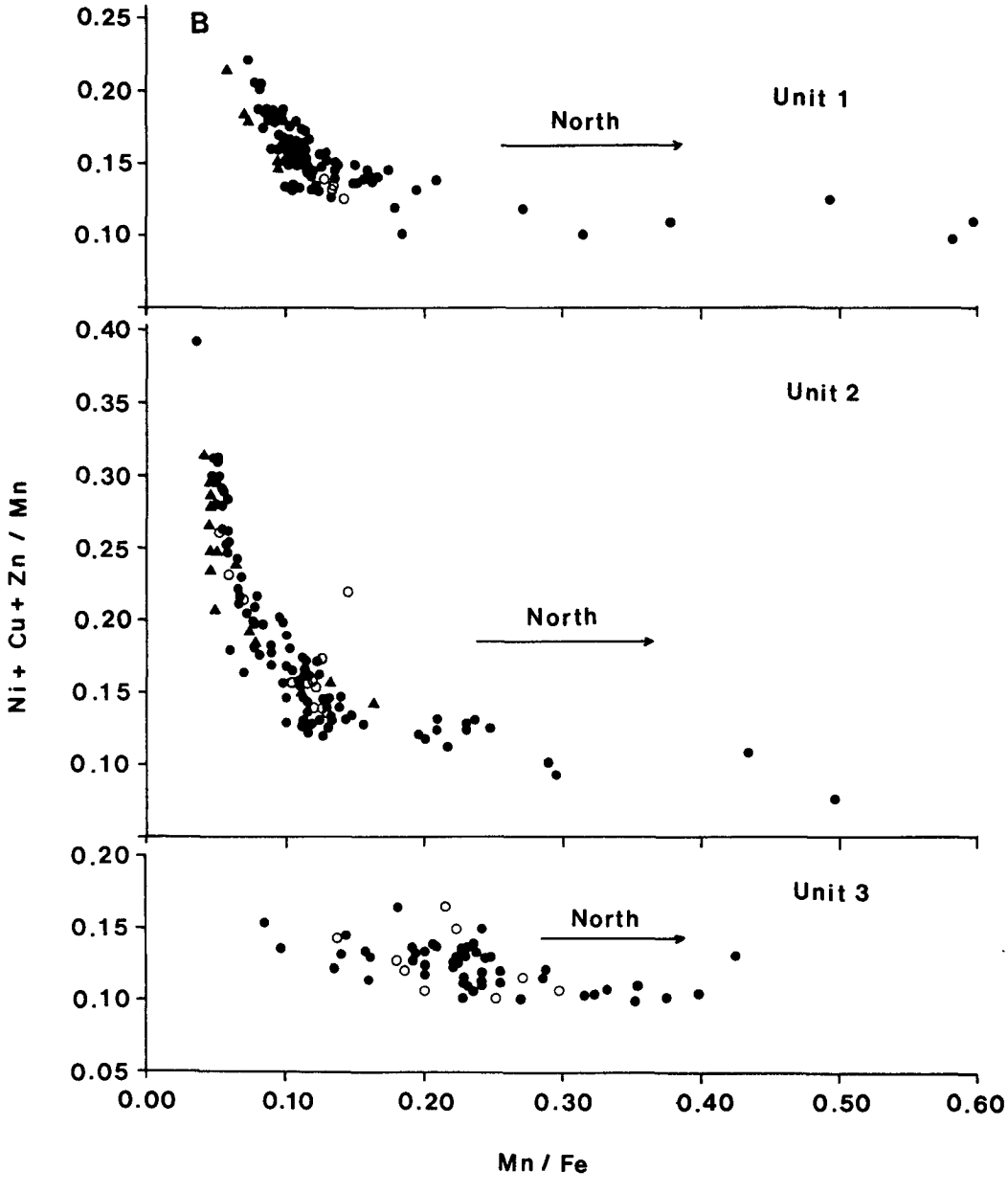

Fig. 20. (continued)

Mn-oxide minerals, nodule types, Mn-crusts, and nodule parts.

	Mineral		Nodule			Mn-crust	Nodule Part		
	Tor (Bus)	Vernadite	R-type	T-type	S-type		Top	Core	Bottom
$I_{10}/I_{2.4}$			0.5-5.4	0.4-4.8	0.3-2.0	57.0-99.0[1]	0.7-4.9	0.0-4.4	0.9-5.5
			(3.0)	(1.9)	(1.3)	(91.5)	(2.8)	(2.5)	(3.6)
Quartz			0.2-6.6	1.0-4.5	0.0-3.7	0.0-2.0	1.2-3.4	0.0-9.9	0.9-4.0
			(2.7)	(2.5)	(1.7)	(0.6)	(2.3)	(2.2)	(1.9)
Feldspar			1.0-24.1	0.0-13.8	0.0-12.4	0.0-26.0	0.0-6.4	0.0-45.6	0.0-5.6
			(6.2)	(4.9)	(3.8)	(2.1)	(2.7)	(9.1)	(2.6)
Phillipsite							0.0-5.3	0.0-54.3	0.0-10.3
							(0.3)	(4.1)	(1.5)
No. of Data			100	24	23	21	17	30	21
Mn	20.1-59.0	7.7 39.7	8.7-29.4	14.4-25.7	14.5-25.0	10.0-26.0	20.1-41.5	10.0-48.6	19.1-45.8
	(40.9)	(23.1)	(22.5)	(21.5)	(20.8)	(22.0)	(26.6)	(25.4)	(28.9)
Fe	0.1-11.2	2.0 31.7	2.6-12.2	4.9-16.1	7.8-18.7	10.4-18.2	4.3-12.9	3.6-16.8	2.3-10.5
	(4.0)	(12.6)	(6.1)	(8.7)	(11.4)	(15.2)	(7.5)	(5.9)	(4.3)
Mn/Fe	2.3-318.6	0.6-11.5	1.5-9.7	1.2-5.2	1.1-2.6	0.9-2.1	1.7-7.5	1.4-13.1	2.0-20.1
	(44.6)	(2.6)	(4.0)	(2.8)	(1.9)	(1.5)	(4.0)	(4.9)	(7.0)
Cu	0.29-2.73	0.09-1.13	0.33-1.67	0.27-1.34	0.11-0.63	0.01-0.37	0.26-1.41	0.18-1.72	0.49-1.53
	(1.60)	(0.51)	(0.97)	(0.72)	(0.47)	(0.12)	(0.84)	(0.92)	(1.20)
Ni	0.73-3.17	0.09-1.63	0.58-1.57	0.50-1.37	0.08-1.28	0.00-0.86	0.52-1.32	0.14-1.29	0.71-1.39
	(1.91)	(0.68)	(1.17)	(1.05)	(0.83)	(0.67)	(0.96)	(0.80)	(1.16)
Cu+Ni	1.17-5.35	0.22-2.76	1.12-3.16	0.77-2.63	0.59-1.91	0.29-1.08	0.78-2.61	0.32-2.96	1.21-2.90
	(3.52)	(1.19)	(2.14)	(1.77)	(1.29)	(0.79)	(1.80)	(1.72)	(2.26)
Co	0.06-0.61	0.05-0.70	0.09-0.79	0.19-0.39	0.20-0.53	0.26-0.62	0.16-0.29	0.03-0.26	0.09-0.28
	(0.23)	(0.31)	(0.21)	(0.25)	(0.31)	(0.53)	(0.22)	(0.15)	(0.16)
Zn	0.00-0.68	0.00-0.16	0.05-0.49	0.08-0.29	0.06-0.19	0.06-0.10	0.09-0.36	0.10-1.15	0.11-0.99
	(0.18)	(0.07)	(0.19)	(0.15)	(0.11)	(0.08)	(0.20)	(0.31)	(0.34)
Growth[2]	4.0-33,822.0	1.2-22.8	2.8-52.8	1.8-15.5	1.5-5.2	0.81-0.93	2.7-19.3		3.4-122.4
Rate	(36.0)	(2.8)	(9.1)	(4.7)	(3.0)	(0.85)	(7.3)		(22.3)
No. of Data :	26	38	161	46	37	21	26	30	30

Tod (Bus), todorokite (buserite); 1, XRD peak intensity; 2, Growth rate = $13.8(Mn/Fe^2) + 0.75$ ($r = 0.95$) (after Huh and Ku, 1984). Averages are in parenthesis.

Table 2a. Interrelation matrix of composition in Mn-oxide minerals.

	Fe			Mn			Ni			Cu			Co			Zn			Si			Al			Mg			Ca			Ti		
	Bulk	T(B)	Vern	Bulk	T(B)	Vern	Bulk	T(B)	Vern	Bulk	T(B)	Vern	Bulk	T(B)	Vern	Bulk	T(B)	Vern	Bulk	T(B)	Vern	Bulk	T(B)	Vern	Bulk	T(B)	Vern	Bulk	T(B)	Vern	Bulk	T(B)	Vern
Mn	-0.33	-0.50*	0.49																														
Ni	-0.71*	-0.56*	-0.60*	0.70*	0.39	0.28																											
Cu	-0.65*	-0.72*	-0.40	0.78*	0.65*	0.30	0.83*	0.54*	0.77*																								
Co	0.29	0.56*	0.09	-0.21	-0.21	0.07	-0.33	-0.35	-0.12	-0.41	-0.47	-0.29																					
Zn	-0.40	-0.50*	0.05	0.51*	0.29*	0.14	0.56*	0.38	0.11	0.63*	0.47	0.33	-0.41	-0.49	-0.24																		
Si	0.58*	0.42	0.60*	-0.02	-0.06	0.25	-0.38	-0.10	-0.45	-0.36	-0.34	-0.12	-0.13	0.08	-0.40	-0.22	-0.26	0.18															
Al	-0.09	-0.06	0.23	0.46	0.33	0.42	0.39	0.37	0.07	0.40	0.22	0.38	-0.23	0.13	-0.40	0.14	-0.13	0.22	0.51*	0.59*	0.75*												
Mg	-0.43	-0.36	-0.14	0.65*	0.49	0.42	0.70*	0.53*	0.55*	0.71*	0.50*	0.77*	-0.25	0.12	-0.52*	0.30	-0.01	0.25	-0.03	-0.28	0.27	0.74*	0.75*	0.71*									
Ca	0.45	0.25	0.83*	0.51*	0.40	0.73*	0.01	-0.14	-0.32	0.11	0.10	-0.24	0.04	0.06	0.11	0.23	0.32	0.04	0.31	0.31	0.47	0.21	0.05	0.25	0.10	-0.03*	0.02						
Ti	-0.02	0.01	0.51*	0.04	-0.07	0.21	-0.00	-0.13	-0.45	0.03	-0.05	-0.49	0.10	0.14	0.77*	-0.06	-0.13	-0.19	-0.04	-0.04	0.03	-0.09	-0.16	-0.10	-0.01	-0.06	-0.51*	-0.03	-0.16	0.44			
P	0.67*	0.62*	0.63*	-0.08	-0.22	0.46	-0.43	0.44	-0.33	-0.39	-0.42	-0.39	0.45	0.44	0.41	-0.20	-0.11	-0.04	0.26	0.26	0.23	-0.12	-0.11	0.00	-0.33	-0.27	-0.25	0.48	0.26	0.66*	0.00	-0.04	0.65*

No. of data set : 64

No. of data : 26 38

Note: T(B) and Vern are abbreviations of todorokite (buserite) and vernadite, respectively. Astericks represent coefficients larger than 0.5.

Table 2b. Interrelation matrix of composition in nodules.

	$I_{10}/I_{2.4}$				Quartz				Feldspar				Mn				Fe				Cu				Ni				Co			
	Bulk	S	R	T	Bulk	S	R	T	Bulk	S	R	T	Bulk	S	R	T	Bulk	S	R	T	Bulk	S	R	T	Bulk	S	R	T	Bulk	S	R	T
Quartz	0.01	0.52*	-0.16	0.34																												
Feldspar	-0.13	0.63*	-0.24	0.21	0.52*	0.63*	0.57*	0.63*																								
Mn	0.51*	-0.01	0.59*	0.57*	-0.21	0.23	-0.13	-0.05	-0.63*	-0.19	-0.52*	-0.27																				
Fe	-0.53*	-0.32	-0.03	-0.21	-0.41	-0.14	-0.01	0.05	-0.42	-0.24	-0.12	-0.12	-0.04	0.53*	0.25	0.19																
Cu	0.70*	0.72*	0.54*	0.88*	0.24	0.71*	0.16	0.28	-0.08	0.39	-0.20	0.20	0.57*	0.45	0.65*	0.69*	-0.73*	-0.24	-0.26	-0.29												
Ni	0.62*	0.45	0.56*	0.69*	0.04	0.53*	-0.08	0.05	-0.29	0.20	-0.40	-0.02	0.71*	0.49	0.80*	0.86*	-0.42	-0.19	0.20	-0.05	0.81*	0.63*	0.72*	0.82*								
Co	-0.19	0.25	0.24	-0.13	-0.29	0.25	0.11	-0.07	-0.36	0.05	0.01	-0.01	0.16	0.51*	0.33	0.27	0.58*	0.52*	0.45	0.67*	-0.33	0.47	0.24	-0.09	-0.13	0.54*	0.29	0.03				
Zn	0.12	0.74*	-0.12	0.78*	0.33	0.48	0.35	0.45	0.22	0.64*	0.23	0.49	0.02	-0.17	0.04	0.31	-0.69*	-0.17*	-0.47	-0.39	0.56*	0.45*	0.42	0.84*	0.24	0.14	-0.02	0.43	-0.55*	-0.02	-0.07	-0.25

No. of Data : 156 26 103 27

Table 2c. Interrelation matrix of composition in Mn-crusts

	$I_{2.4}$	Quartz	Feldspar	Mn	Fe	Cu	Ni	Co
Quartz	-0.32				No.of Data : 21			
Feldspar	-0.85*	0.49						
Mn	0.77*	-0.12	-0.76*					
Fe	0.63*	-0.03	-0.33	0.28				
Cu	0.46	-0.11	-0.27	0.21	0.66*			
Ni	0.30	-0.18	-0.41	0.35	0.20	0.21		
Co	0.46	0.13	-0.32	0.66*	0.05	-0.03	-0.06	
Zn	0.30	-0.17	-0.36	0.19	0.36	0.61*	0.27	0.03

Table 3. Chemical composition of selected smectite and Mn-micronodules in box core sediments.

Smectite	Core No. K9037 1 cm depth	20 cm	40 cm
Fe (%)	8.0	8.7	4.7
Mn (PPM)	180.0	200.0	387.7
Ni (PPM)	206.7	166.7	340.0
Cu (PPM)	306.7	300.0	573.3
Co (PPM)	56.0	80.0	266.7
Mn-micronodule	**Core No. K9034 4 cm depth**		**Core No. K9025 25 cm depth**
Fe (%)	7.7		8.3
Mn (%)	27.0		25.0
Ni (%)	1.1		0.8
Cu (%)	1.3		0.7
Co (%)	0.2		0.3

Table 4. Interrelation matrix of sediment constituents.

	Fe	Mn	Mn/Fe	Cu	Ni	Co	Zn	Smectite	Illite
Mn	0.28								
Mn/Fe	-0.22	0.85*			No. of data : 148				
Cu	0.40	0.85*	0.62*						
Ni	0.37	0.87*	0.70*	0.72*					
Co	0.65*	0.56*	0.22	0.72*	0.50*				
Zn	0.62*	0.77*	0.42	0.83*	0.75*	0.63*			
Smectite	-0.38	0.27	0.44	0.23	0.05	0.16	0.13		
Illite	0.38	-0.26	-0.43	-0.23	-0.03	0.15	-0.12	-0.99*	
K+C	0.37	-0.27	-0.43	-0.23	-0.11	0.17	-0.14	-0.94*	0.89*

K+C : Sum of kaolinite and chlorite
Asterick represents correlation coefficient larger than 0.5.